

Master 1 Physique fondamentale et applications

Internship's report
April-August 2023

Far-Off resonance laser locking

Corentin Morin

LKB Paris

Directed by Quentin Glorieux



Contents

1	Introduction	3
2	The Rb system and fluidity of light	3
2.1	The Rubidium atom and its energy levels	3
2.2	Electric susceptibility of a two level system	3
2.3	Paraxial fluid of light	5
3	How to lock a laser?	5
4	Far off resonance laser locking methods	6
4.1	Atoms in a magnetic field	6
4.2	The Faraday Effect	8
4.3	The DAVLL lock	11
5	The magnetic field generation	11
6	Evaluating the stability of the zero crossings of the Faraday effect	13
6.1	A tool, the Allan variance	13
6.2	Experimental setup	14
6.3	Results	16
7	First locks stability	17
7.1	Experimental setup	17
7.2	Results	17
8	Tuning the zero crossings	18
8.1	Using a linear actuator to move the magnets	18
8.2	Setting the desired lock point	19
9	Embedding the Faraday lock system in a box	21
10	Conclusion	22
A	Side activities	23
A.1	Designing holders for the magnets	23
A.2	Home made balanced photo-diodes	23
A.3	GPIB to USB — Interfacing the Spectrum Analyzer	23
A.4	Developping a python controlled continuous linear actuator	23
A.5	TENMA power source interface	23
A.6	Installing a router in the Rb room	23
B	Cell's temperature determination	23

1 Introduction

The Quantum optics group at LKB Paris works on Quantum Fluids of Light. When light goes through a non-linear medium, photons can be seen as interacting together, this interaction is mediated by the non-linear medium. In the Rubidium team of the group, the non-linear medium is a hot gas of rubidium atoms. The nature of the non linear interaction pushes the group to work at precise frequencies and especially frequencies off resonance with the energies of the atoms of the gas.

The goal of this internship was to develop a system allowing the group to lock in frequency the lasers used out off resonance. In order to do so, we chose to use the properties of the atomic energies when the gas experiences a magnetic field.

In this report we present the work made during this internship, especially the theory and the stabilization characterizations of the system.

2 The Rb system and fluidity of light

2.1 The Rubidium atom and its energy levels

The Rubidium atom is an alkali. It's atomic number is $Z = 37$. It has two stable isotopes : the ^{85}Rb and the ^{87}Rb . Its electronic ground state is $[Kr]5s^1$. It correspond to a $5^2S_{1/2}$ level in L-S coupling (arising from the electrostatic interactions between the electrons). [1]. The two first excited states arise from the electronic state $[Kr]5p^1$ which corresponding levels in L-S coupling are $5^2P_{1/2}$ and $5^2P_{3/2}$. The transition $5^2S_{1/2} \rightarrow 5^2P_{1/2}$ is called the D1 line (centered around 795 nm for both isotopes) and the transition $5^2S_{1/2} \rightarrow 5^2P_{3/2}$ is called the D2 line (centered around 780 nm for both isotopes). By taking the interactions with the nuclear spin which equals 5/2 for the ^{85}Rb and 3/2 for the ^{87}Rb , the levels precedently cited split into hyperfine levels. [2][3] The D2 and D1 lines energy levels are presented below in figure 2.1.1.

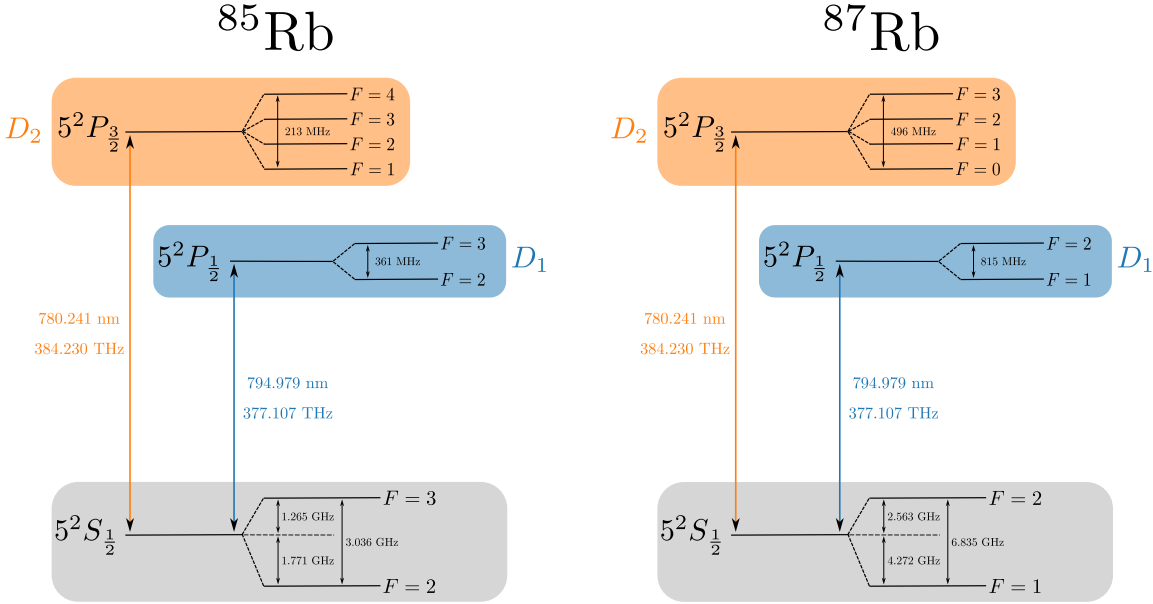


Figure 2.1.1: Energy levels in L-S coupling and with the hyperfine levels for a) ^{85}Rb and b) ^{87}Rb — Figure made by Tangui Aladjidi

2.2 Electric susceptibility of a two level system

In order to understand the interaction of the rubidium atoms in the hot atomic vapor with the light passing through it, we will model our atoms by a two level system. The polarizability of the medium will thus be written as $P(\vec{\omega}) = \epsilon_0 \chi(\omega) E(\vec{\omega})$, with ϵ_0 being the void's permittivity, $\chi(\omega)$ the electric susceptibility of the medium, $E(\vec{\omega})$ the electric field of the light passing through the medium. Then, we can write the electric displacement field $D(\vec{\omega}) = \epsilon_0 E(\vec{\omega}) + P(\vec{\omega})$. By using the Maxwell equations, the wave vector in the middle then writes $k_{Rb} = k_{void} \times \sqrt{1 + \chi(\omega)}$ with k_{void} being the wave vector in the void. We then define the absorption coefficient $\alpha(\omega) = Im(\sqrt{1 + \chi})$ and the refractive index of the middle $n(\omega) = Re(\sqrt{1 + \chi})$ [4].

Now we must find the expression for $\chi(\omega)$, this is done by writing the optical Bloch equations and by introducing the processes for the relaxation [5]. By the end, we get :

$$\chi(\omega) = \frac{\alpha_0(0)}{\omega_{eg}/c} \frac{i - \Delta/\gamma}{1 + (\frac{\Delta}{\gamma})^2 + (\frac{E_0}{E_s})^2} \quad (2.2.1)$$

Here, $\alpha_0(0)$ corresponds to the absorption coefficient at resonance, ω_{eg} is the Bohr pulsation of the atomic transition, Δ is the detuning between the Bohr pulsation of the atomic transition and the pulsation of the electric field ω , γ is equal to half the spontaneous emission rate, E_0 is the electric field amplitude and E_s is the saturation field strength. A visualization of the absorption coefficient and the refractive index is shown in figure 2.2.1.

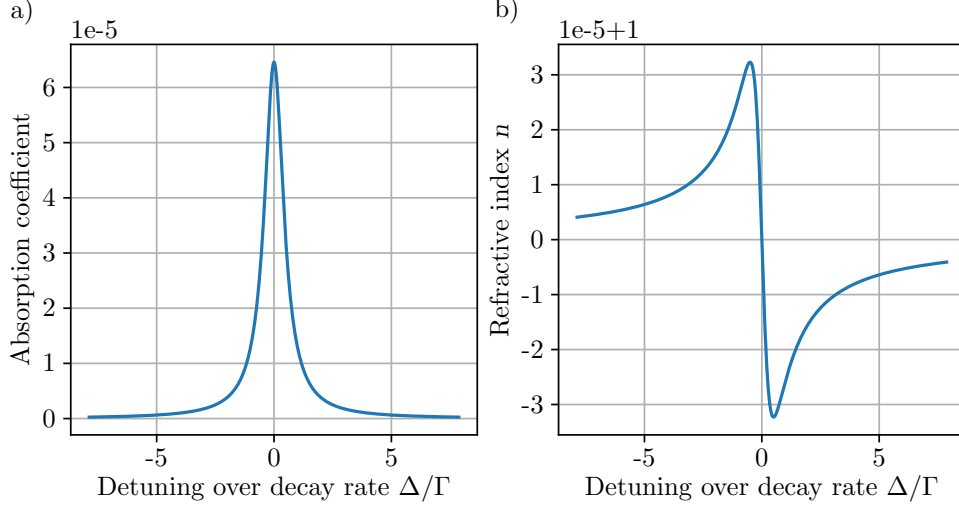


Figure 2.2.1: a) Absorption coefficient of a two level system, b) Refractive index of a two level system

It is important to notice that far off resonance the absorption coefficient evolves as $1/\Delta^2$ while the refractive index of the medium evolves as $1/\Delta$, Δ being the detuning from the energy of the resonant transition.

When $E_0 \ll E_s$, it is possible to realize a serie expansion on $\chi(\omega)$ such that $\chi(\omega) = \chi^{(1)}(\omega) + \frac{3}{4}\chi^{(3)}(\omega)E_0^2$ [6] (see equation 2.2.2).

$$\chi(\omega) = \frac{\alpha_0(0)}{\omega_{eg}/c} \left(1 - \left(\frac{E_0}{E_s}\right)^2 \frac{1}{1 + (\frac{\Delta}{\gamma})^2}\right) \quad (2.2.2)$$

Then, the refractive index can be written $n = n_0 + n_2 I$, I being the intensity of the electromagnetic field. n_2 is the non-linear refractive index of the medium. The calculations show that $n_2 = \frac{3}{4} \frac{Re(\chi^{(3)})}{\epsilon_0 n_0^2 c}$, $n_0 = \sqrt{1 + Re(\chi^{(1)})}$ and $I = n_0 c \frac{1}{2} \epsilon_0 E_0^2$ [7]. A comparison of $Re(\chi^{(1)})$ and $Re(\chi^{(3)})$ is presented in figure 2.2.2.

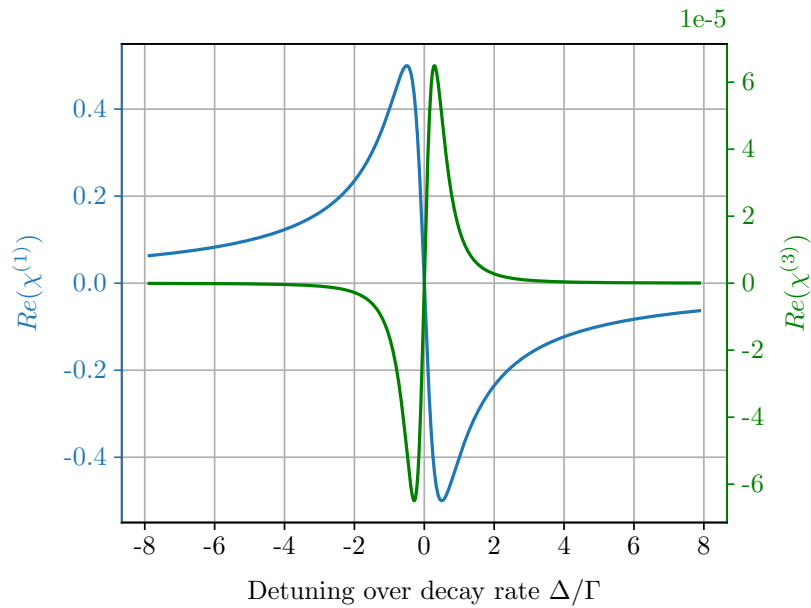


Figure 2.2.2: Comparison of the linear electric susceptibility vs. the second order electric susceptibility

2.3 Paraxial fluid of light

If we let an electric field written as $\vec{E} = E(r_{\perp}^{\vec{z}}, z)e^{ik_0 \vec{e}_z \cdot \vec{r}} \vec{e}$, propagate along the z direction in a non linear medium (a medium of which the refractive index depends on the intensity of the electromagnetic field passing through it), under some approximations we can find, using the Maxwell equations an equation of evolution for the electric field called the Non Linear Schrödinger Equation (NLSE) [6]. One of these approximations is the paraxial approximation stating that the characteristic length on which the amplitude of the electric field $E(r_{\perp}^{\vec{z}}, z)$ evolves in the z direction is much larger than the optical wavelength of the light propagating. The NLSE is presented in figure 2.3.1.a). The notation are those introduced precedently with $\delta\epsilon(r)$ being a tiny modulation of the electric permittivity $\epsilon = 1 + \chi$.

a)

Non-linear Schrödinger equation :
propagation with intensity dependent refractive index

$$i \frac{\partial}{\partial z} E = \left(\underbrace{-\frac{1}{2k_0} \nabla_{\perp}^2}_{\text{kinetic energy}} - \underbrace{\frac{\delta\epsilon(\mathbf{r})}{2n_0} k_0}_{\text{external potential}} + \underbrace{i \frac{\alpha}{2}}_{\text{losses}} - \underbrace{\frac{n_2}{n_0} k_0 |E|^2}_{\text{non-linear interaction}} \right) E$$

b)

Gross Pitaevskii Equation :
description of an interacting Bose gas

$$i \hbar \frac{\partial}{\partial t} \psi = \left(\underbrace{-\frac{\hbar^2}{2m} \nabla^2}_{\text{kinetic energy}} + \underbrace{V}_{\text{external potential}} + \underbrace{i \hbar \frac{\gamma}{2}}_{\text{losses and pumping}} + \underbrace{g |\psi|^2}_{\text{non-linear interaction}} \right) \psi$$

Figure 2.3.1: a) Non-linear Schrödinger equation, b) Gross Pitaevskii equation — Figure extracted from the group material

The NLSE can be reformulated using an hydrodynamic formulation. Let's write $E = |E|(r_{\perp}^{\vec{z}}, z)e^{i\phi(r_{\perp}^{\vec{z}}, z)}$. The NLSE then describes the propagation of a fluid of light with the density of the fluid being $\rho(r_{\perp}^{\vec{z}}, z) = |E(r_{\perp}^{\vec{z}}, z)|^2$ and the speed of the fluid being $\vec{v}(r_{\perp}^{\vec{z}}, z) \propto \nabla\phi(r_{\perp}^{\vec{z}}, z)$.

As shown in figure 2.3.1, an analogy can be made between the NLSE and the equation governing the time evolution of the ground state wave function of an interacting Bose gas, the Gross Pitaevskii equation [8][6]. The fluid of light is analogous to a gas of interacting photons. The 2D map of the electric field at a position z is analogous to the wave function of a 2D Bose gas at a time t . The propagation of the electric field is thus similar to the time evolution of 2D Bose gas. The kinetic energy of the fluid of light is mapped into the transversal gradient of the electric field. Applying a modulation to the permittivity of the non-linear medium is equivalent to applying a potential to the fluid of light. The losses in the photon gas are linked to the optical absorption of the non linear medium. Finally the coupling constant g characterizing the effective interactions in the photon gas is equal to $-\frac{n_2}{n_0} k_0$.

In order for a Bose gas to be stable, the coupling constant g must be positive [8] which means, that in our system, n_2 must be negative. We saw previously that n_2 has the same sign than $Re(\chi^{(3)})$. According to figure 2.2.2, we must then work at negative detunings. In order to avoid the effects of absorption, we will work off resonance.

We must then need a tool to lock the frequency of the lasers off resonance in order to study the physics of fluids of light.

3 How to lock a laser?

In order to lock the frequency of a laser, we need to know its frequency thanks to a reference. In our case we needed an absolute reference in order for our system to be standalone. We are using a Rubidium gas as our reference. Indeed, as every atom has the same properties, we can extract the frequency of the laser light by studying the effect of the atoms on its propagation.

From the reference, we need to be able to extract an error signal, typically an electronic signal. This error signal should be linear around the desired frequency lock point and equal to zero at this exact frequency. Thus, this error signal is proportional to the difference between the actual frequency and the lock point.

The error signal will allow us to counter-react on some parameters of the lasers. For example, on diode laser we can counter-react on the current alimenting the diode or the length of the laser cavity by applying a voltage to a piezo-electric actuator. The magnitude of the counter-reaction and its sign are determined by the error signal.

This working principle is presented in figure 3.0.1.

This work will focus on the generation of the error signal for a tunable off resonance locking system for negative frequencies detuning. Typically, in this work we will take the D2, F=2 (ground state) ^{87}Rb transition as the frequency detuning reference.

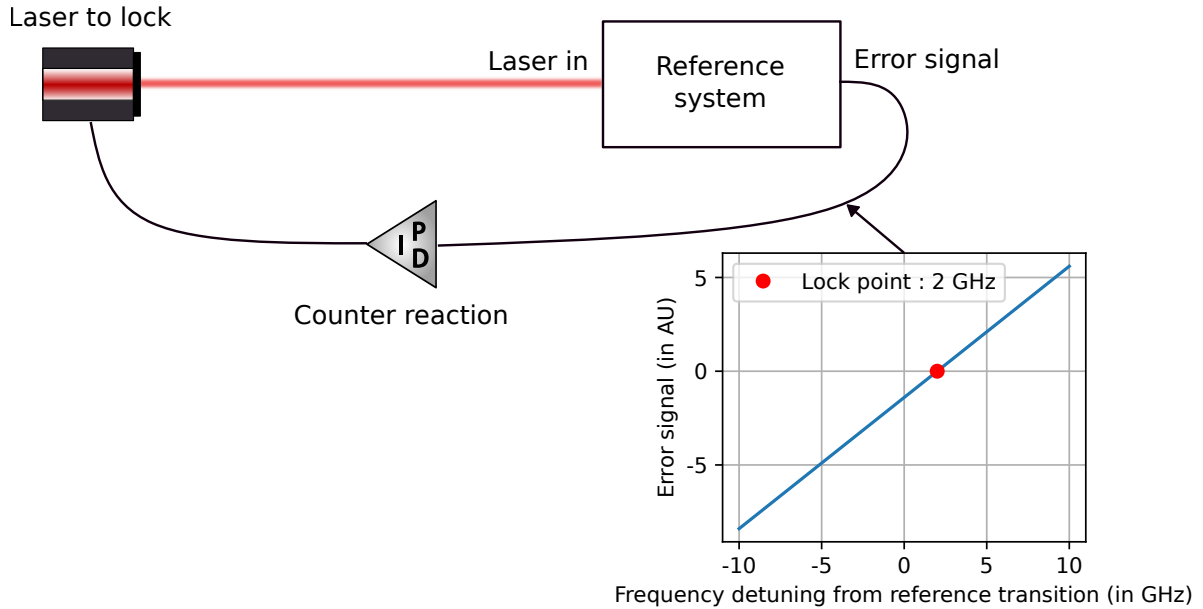


Figure 3.0.1: Working principle of a laser frequency locking system

4 Far off resonance laser locking methods

We will now examine how we can generate an off resonance error signal.

4.1 Atoms in a magnetic field

Plunging our atoms in a magnetic field can be of great use for our locking system. Thus we must understand the effects of the magnetic field on the atoms.

4.1.1 Hamiltonian and perturbed energy

When an atom experiences a magnetic field the energies of some levels will shift and some degeneracies will be lifted. The Hamiltonian of an atom in a magnetic field can be written $H = H_0 + H_{hf} + H_Z$ with H_0 being the Hamiltonian of a free atom (with fine structure effects), H_{hf} being the hyperfine structure Hamiltonian and $H_Z = -\vec{B} \cdot (\vec{M}_S + \vec{M}_L + \vec{M}_I)$ being the Zeeman Hamiltonian with \vec{B} being the magnetic field along the z-axis, \vec{M}_L the magnetic moment associated to the electron angular momentum, \vec{M}_S the magnetic moment associated to the electron spin and \vec{M}_I the magnetic moment associated to the nuclear spin. [9].

According to the amplitude of the applied magnitude field we can distinguish two main regimes.

First, for weak fields ($\langle H_z \rangle \ll \langle H_{hf} \rangle$), H_Z is treated as a perturbation of $H_0 + H_{hf}$. The eigen states are $|n, L, S, I, F, m_F\rangle$, with n being the principal quantum number, L the electron angular momentum quantum number, S the electron spin quantum number, I the nuclear spin quantum number, F the total atomic angular momentum quantum number and m_F the total atomic angular momentum projection quantum number. The energy splitting can be written $\Delta E(m_F, B_z) = B_z \times \mu_B \times g_F \times m_F$ with B_z being the amplitude of the magnetic field, μ_B the Bohr magneton, and g_F the hyperfine Landé factor. This is called the normal Zeeman effect. [2][3]

For strong fields ($\langle H_{hf} \rangle \ll \langle H_z \rangle$), H_{hf} needs to be treated as a perturbation of $H_0 + H_Z$. The eigen states are $|n, L, S, J, m_J\rangle \otimes |I, m_I\rangle$ with J being the total electron angular momentum quantum number, m_J the total electron angular momentum projection quantum number and m_I the nuclear spin projection quantum number. The energy splitting can be written $\Delta E(m_J, m_I, B_z) = B_z \times \mu_B \times (g_J \times m_J + g_I \times m_I)$ with g_J being the fine structure Landé factor and g_I the nuclear Landé factor. This is called the anomalous Zeeman effect or the Paschen-Back effect. [2][3]

The effect of a magnetic field on the $^{87}\text{Rb } 5^2S_{1/2}$ hyperfine levels is represented in figure 4.1.1. We clearly see the two regimes.

4.1.2 Effect of the magnetic field on the observed transitions

When an atom experiences light, in the first order, the interaction of this atom with the electromagnetic field reduces to the interaction of its dipolar moment with this electric field. Our atoms experiencing also a magnetic field, their axis of quantification is set along the direction of this magnetic field.

The selection rules, dictating the levels that can be coupled through the interaction with an electric field can then be deduced through a perturbative approach [9].

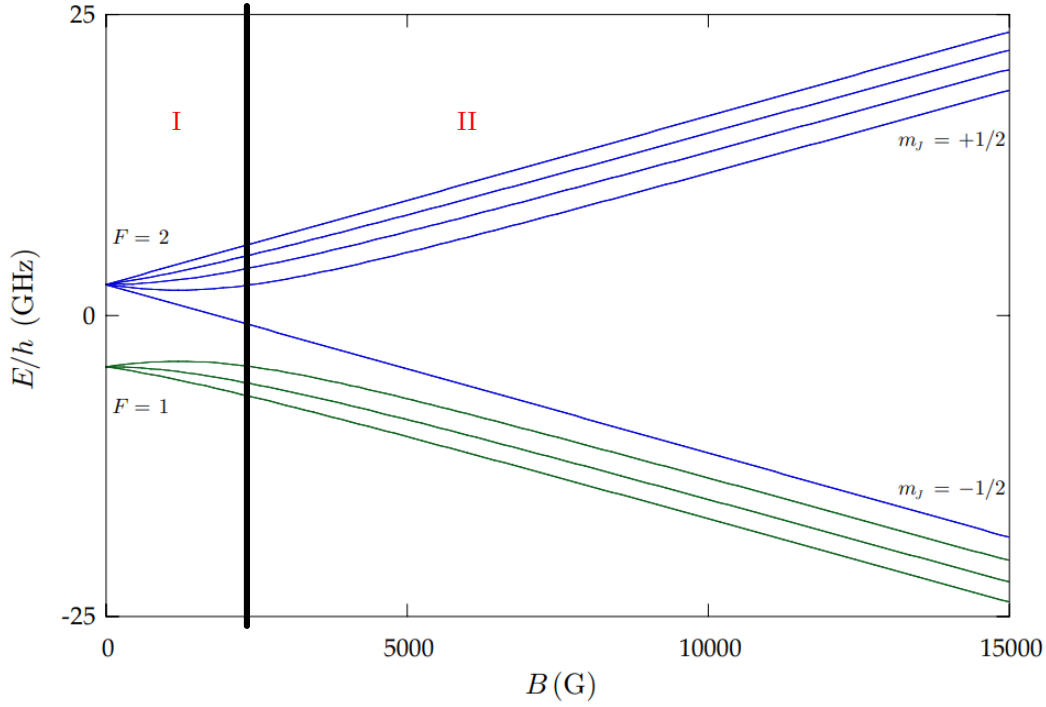


Figure 4.1.1: Zeeman splitting of the $^{87}\text{Rb } 5^2S_{1/2}$ level under a magnetic field B . I/ Normal Zeeman effect, II/ Anomalous Zeeman effect — Figure adapted from [3]

In the following we will index with a g the ground state and with a f the final state of an authorized transition induced by the electric field. Let's cite the selection rules for the two basis we saw earlier :

- For a right handed circularly polarized light, noted σ^+ (see red arrows in figure 4.1.2):
 - In the $|n, L, S, J, m_J\rangle \otimes |I, m_I\rangle$ basis, $n_g = n_f, L_f = L_g \pm 1, S_f = S_g, J_f = J_g$ or $J_f = J_g \pm 1, m_{Jf} = m_{Jg} + 1, I_f = I_g, m_{If} = m_{Ig}$ (conservation of the nuclear spin)
 - In the $|n, L, S, I, F, m_F\rangle$ basis, $n_g = n_f, L_f = L_g \pm 1, S_f = S_g, I_f = I_g, F_f = F_g$ or $F_f = F_g \pm 1, m_{Ff} = m_{Fg} + 1$
- For a left handed circularly polarized light, noted σ^- (see blue arrows in figure 4.1.2):
 - In the $|n, L, S, J, m_J\rangle \otimes |I, m_I\rangle$ basis, $n_g = n_f, L_f = L_g \pm 1, S_f = S_g, J_f = J_g$ or $J_f = J_g \pm 1, m_{Jf} = m_{Jg} - 1, I_f = I_g, m_{If} = m_{Ig}$ (conservation of the nuclear spin)
 - In the $|n, L, S, I, F, m_F\rangle$ basis, $n_g = n_f, L_f = L_g \pm 1, S_f = S_g, I_f = I_g, F_f = F_g$ or $F_f = F_g \pm 1, m_{Ff} = m_{Fg} - 1$

These selection rules can be understood as a conservation of the "total angular momentum" of both the incoming photon and the atom. They are illustrated in figure 4.1.2. They are also true when no splitting exists between the levels.

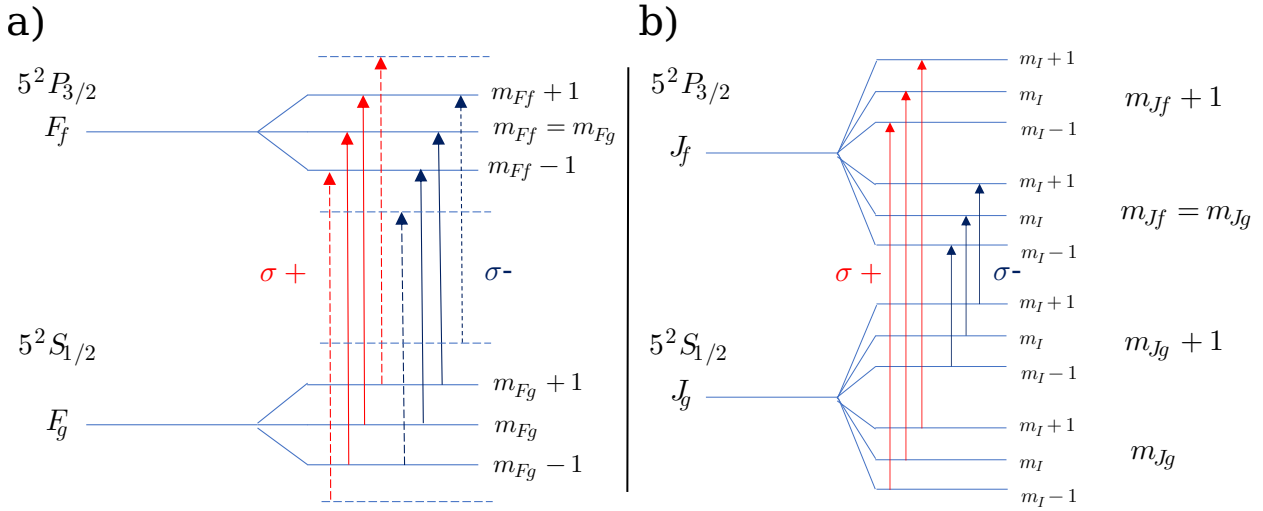


Figure 4.1.2: a) Selection rules for transitions under an electric field in the $|n, L, S, I, F, m_F\rangle$ basis, b) Selection rules for transitions under an electric field in the $|n, L, S, J, m_J\rangle \otimes |I, m_I\rangle$ basis — The levels are splitted as if a magnetic field was applied

4.1.3 Dichroism

The energy of the transition ($\Delta E = E_f - E_g$) being shifted by the magnetic field we see dichroism appearing in the absorption spectrum.

Let's consider the $^{85}\text{Rb } 5^2S_{1/2}, |J = 1/2, m_{Jg} = 1/2\rangle \rightarrow 5^2P_{3/2}, |J = 3/2, m_{Jf} = m_{Jg} \pm 1\rangle$ transition with an excitation light in both left and right handed circularly polarized light.

On the left side of figure 4.1.3 we see that the optical index and the absorption coefficient of the atom are centered around the detuning we set to be zero where the absorption coefficient is maximum. When we apply a magnetic field of 1.4kG, the transitions arising from the left circularly polarized and the right circularly polarized light split. This is dichroism.

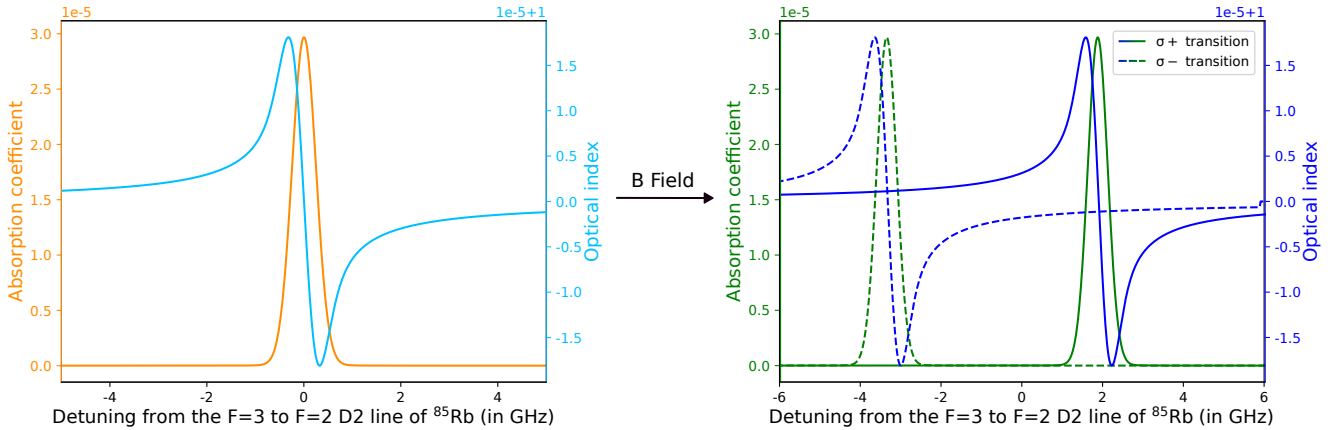


Figure 4.1.3: On the left (right) are represented the absorption coefficient and the optical index for the $5^2S_{1/2}, |J = 1/2, m_J = 1/2\rangle \rightarrow 5^2P_{3/2}, |J = 3/2, m_F = 3/2\rangle$ of a ^{85}Rb atom — We are in the strong field regime because the magnetic field applied is of 1.4kG

4.2 The Faraday Effect

4.2.1 Presentation and theory

The Faraday effect [10] [11] is an effect arising from the dichroism induced by a magnetic field, it rotates the polarization of light. It is based on the splitting of the optical indexes of the circularly polarized transitions. It only works off-resonance where the effect of the absorption gets negligible before the effects of the dispersion of the middle, that is to say when the frequency detuning is larger than the inverse of the life time of the considered transition (see part 2.2).

Let's consider the system presented in figure 4.2.1. The laser light coming out from the laser is linearly polarized. We rotate the polarization with a lambda half plate such that the electric field entering the rubidium cell can be written $E_{in}(\omega) = \frac{1}{\sqrt{2}}|E_{in}(\omega)|(\vec{e}_x + \vec{e}_y)$ where \vec{e}_x and \vec{e}_y are the polarization axis defined by the polarizing beam

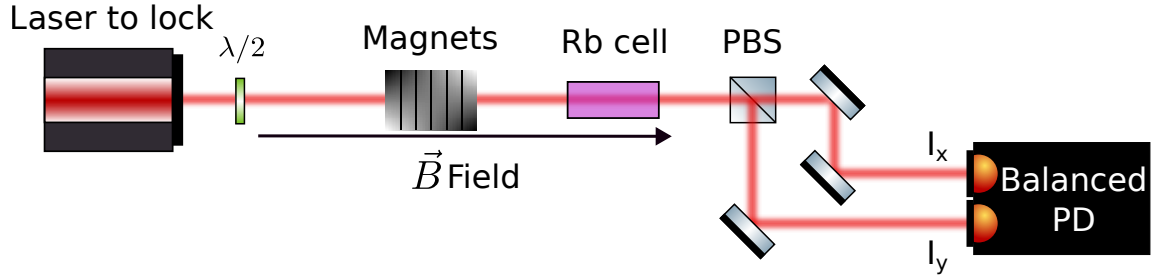


Figure 4.2.1: Experimental setup for the Faraday effect

splitter. As we know, $e_+^- = \frac{1}{\sqrt{2}}(e_x^- + ie_y^-)$ and $e_-^- = \frac{1}{\sqrt{2}}(e_x^- - ie_y^-)$ with e_+^- (respectively e_-^-) being the unit vector for the right (respectively left) handed circular polarization.

As seen previously, the contributions for the absorption and the dispersion induced by opposite circularly polarized light are not the same. Thus in order to know the electric field at the output of the cell, E_{out} , we must separate the contributions such that as presented in the equation 4.2.1 (we consider $k_{void} \cdot u_{cell} L = kL$, meaning the cell is aligned with the direction of propagation of light, and we note $|k_{void}| = k$):

$$E_{out}^-(\omega) \cdot e_{\pm}^- = E_{in}^-(\omega) \cdot e_{\pm}^- \times e^{-\alpha_{\pm}(\omega)kL} \times e^{in_{\pm}(\omega)kL} \quad (4.2.1)$$

Thus, we get after the polarizing beam splitter:

$$\begin{aligned} E_{out}^- \cdot e_x^- &= \frac{1}{2}(E_{out}^- \cdot e_+^- + E_{out}^- \cdot e_-^-) \\ E_{out}^- \cdot e_y^- &= \frac{-i}{2}(E_{out}^- \cdot e_+^- - E_{out}^- \cdot e_-^-) \end{aligned} \quad (4.2.2)$$

Finally, with $\Delta\alpha(\omega) = \alpha_+(\omega) - \alpha_-(\omega)$ and $\Delta\phi(\omega) = (n_+(\omega) - n_-(\omega))kL$

$$\begin{aligned} I_x &\propto |E_{out}^- \cdot e_x^-|^2 \propto e^{-2\alpha_+(\omega)kL} + e^{-2\alpha_-(\omega)kL} + e^{-\Delta\alpha(\omega)kL} e^{i\Delta\phi(\omega)} + e^{\Delta\alpha(\omega)kL} e^{-i\Delta\phi(\omega)} \\ I_y &\propto |E_{out}^- \cdot e_y^-|^2 \propto e^{-2\alpha_+(\omega)kL} + e^{-2\alpha_-(\omega)kL} - e^{-\Delta\alpha(\omega)kL} e^{i\Delta\phi(\omega)} - e^{\Delta\alpha(\omega)kL} e^{-i\Delta\phi(\omega)} \\ I_x - I_y &\propto e^{-\Delta\alpha(\omega)kL} e^{i\Delta\phi(\omega)} + e^{\Delta\alpha(\omega)kL} e^{-i\Delta\phi(\omega)} \end{aligned} \quad (4.2.3)$$

We can simplify the output of the balanced photo-diode $I_x - I_y$ 4.2.3 for frequency detunings larger than the inverse of the life time of the considered transition such that $\Delta\alpha(\omega) = 0$, because as seen precedently the absorption coefficient α goes faster to zero than the optical index goes to 1, then :

$$I_x - I_y \propto \cos(\Delta\phi(\omega)) \quad (4.2.4)$$

The Faraday effect allows us to probe the dispersion difference, thus the phase difference between the two circular polarisations of light as we see in equation 4.2.4.

A cosine having multiple zero crossings and being almost linear near these zero crossings (assuming the phase difference between the two circular polarizations of light to be continuous), the difference between the optical intensities in the vertical and in the horizontal polarisations can be a good candidate for a frequency locking error signal.

A simulation (see figure 4.2.2.a)) and an experimental observation (see figure 4.2.2.b)) of the Faraday effect are presented in figure 4.2.2. Around the zero detuning, the Faraday signal is equal to zero because of the strong absorption of the heated cell. We can observe multiple zero crossings before the phase difference between the two polarisations (horizontal and vertical) vanishes. These are our lock points.

4.2.2 The different parameters for the positions of the zero crossings

In order to be able to tune the frequency position of our lock points we must find parameters we can play with.

By tuning the magnetic field applied to the cell, we then modify the splitting between the opposed polarization transitions. This results in a modification of the Faraday signal. A simulation of how a Faraday signal can change with this splitting is presented in figure 4.2.3.

Modifying the magnetic field is simple. Indeed, it as been observed experimentally that the magnetic field doesn't have to be homogeneous to get an exploitable Faraday signal (the signal presented in 4.2.2.b) is obtained with an inhomogeneous field). A short study of the field applied is presented in part 5. Thus, in order to modify the magnetic field we can play on the distance between the cell and the magnetic field source.

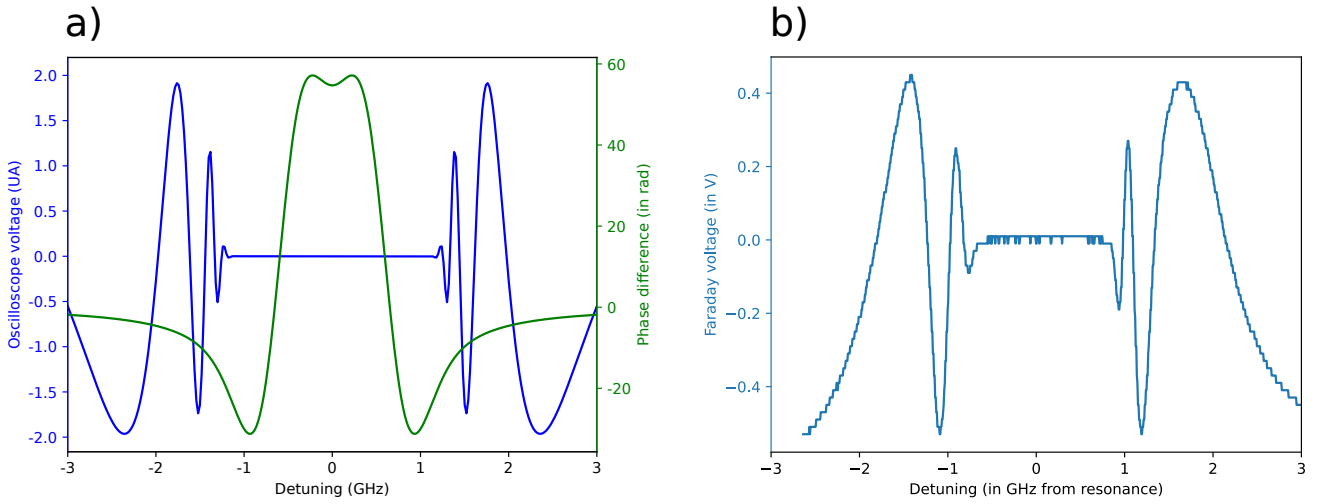


Figure 4.2.2: a) Simulation of the Faraday effect for a splitting between the transitions of 600 MHz, in green we can see the phase difference between the two polarizations which causes the Faraday effect, b) An experimental observation of the Faraday effect around the D2, F=2 transition of ^{87}Rb , in a pure ^{87}Rb cell of 5cm long heated at 100°C under an inhomogeneous magnetic field with a maximum of 1.4kG

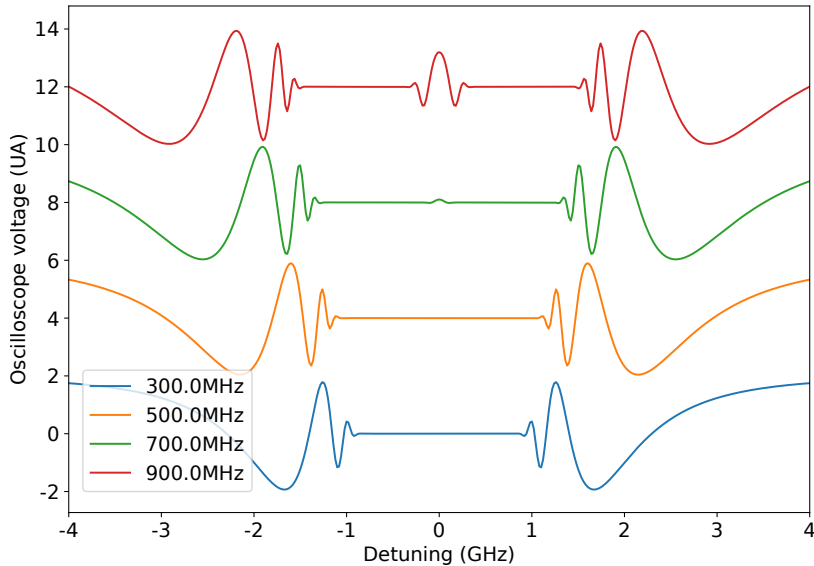


Figure 4.2.3: Simulation of the Faraday effect for different splittings (given in the legend) between the left and right circularly polarized light with a fixed temperature of 105°C

An other effect, that can be problematic [10] is the effect of the temperature of the cell. The results of simulations for the positions in frequency of the zero crossings for different temperatures are shown in figure 4.2.4.

These changes in the Faraday effect due to temperature changes come from the fact that with the temperature, the electric susceptibility gets higher and wider. This effect is both interesting and problematic. Indeed, in order to get a stable Faraday signal we must achieve to get low temperature variations. But, as we see in figure 4.2.4, with the same range of accessible magnetic fields, by tuning the temperature, we tune the lock point range of the system.

The simulated system is a two-level system only, then the simulations are just indicative. Nevertheless, these simulations can give us an idea of the order of magnitude of the effect of the temperature on our system. The gradients of the positions in frequency of the three first zero crossings presented in figure 4.2.4.b) are presented in figure 4.2.5. We see that the positions of the zero crossings move by around $10\text{MHz}/^\circ\text{C}$ which confirms the impact of the temperature stability over the stability of the frequency detuning of the zero crossing and thus the stability of our lock.

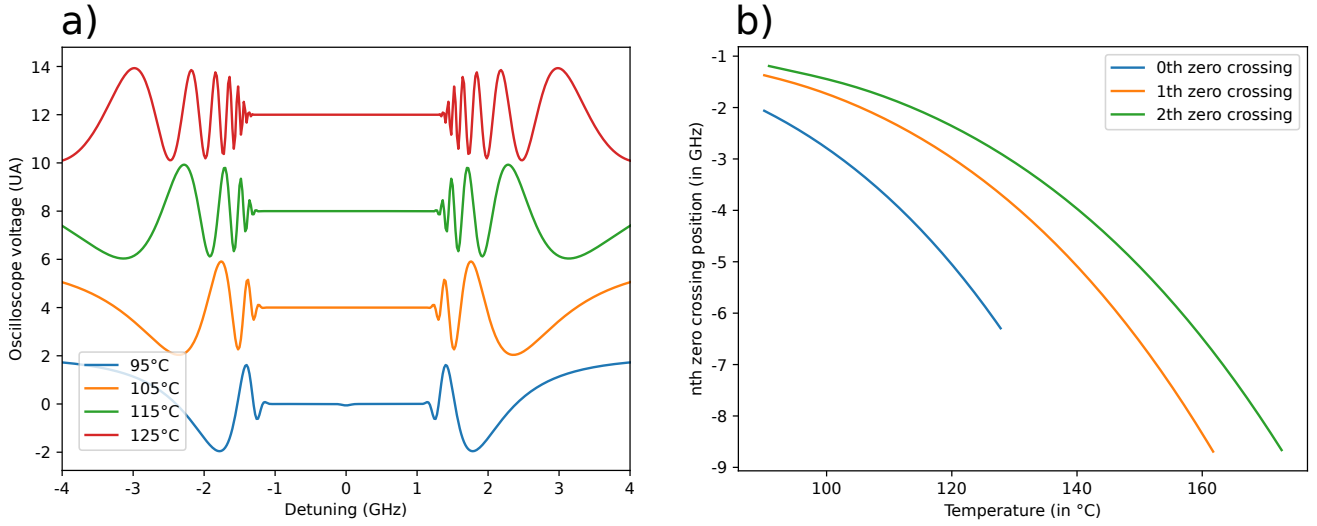


Figure 4.2.4: a) Simulation of the Faraday effect for different temperatures with a fixed splitting of 600MHz between the left and right circularly polarized light, b) Tracking of the positions of the three first zero crossings of the simulations of the Faraday effect for different temperatures with a fixed splitting of 600MHz between the left and right circularly polarized light

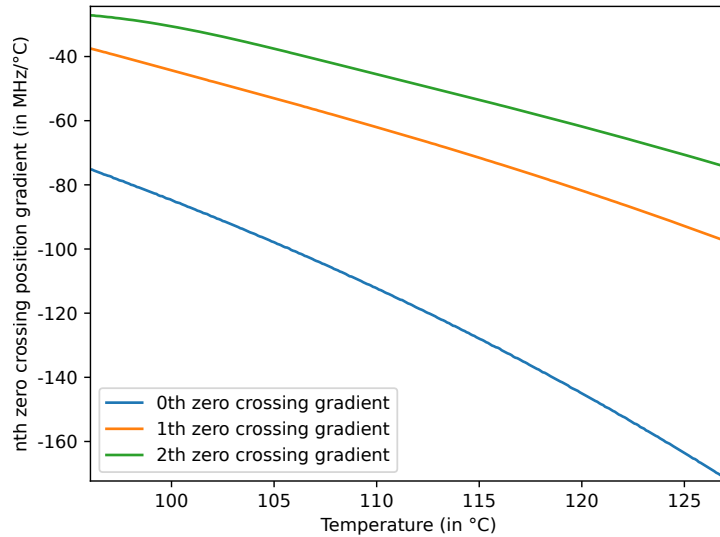


Figure 4.2.5: Gradient of the position in frequency of the zero crossings presented in figure 4.2.4.b)

4.3 The DAVLL lock

An other way to lock far off resonance is the DAVLL lock (Dichroic Atomic Vapor Laser Lock) [12] [13] [14] [15]. Instead of exploiting the dichroism in the optical index, it exploits the dichroism in the absorption coefficient in order to obtain a linear error signal around the lock point.

5 The magnetic field generation

Presentation of the magnets

For generating the magnetic field we chose to use magnets. The magnets used to generate the magnetic field (see figure 5.0.1.a)) were bought from <https://www.supermagnete.gr/>. They are magnets with a hole with poles aligned according to the cylinder axis 5.0.1.b).

We ran simulations with the python library *Magpylib* [16] in order to calculate the magnetic field produced by the magnets. But the magnetic field produced by ring magnets can be seen as the magnetic field created by a tiny solenoid (of the inner diameter of the ring magnet) inside a wider solenoid (of the external diameter of the ring magnet) with the same height and opposed currents [17][18].

For one magnet, the magnetic field map is presented in 5.0.2.a). A cut along the cylindrical axis of this map is presented in figure 5.0.2.b). The values of the magnetic field were multiplied by a coefficient in order to fit the experiment that will be shown next.

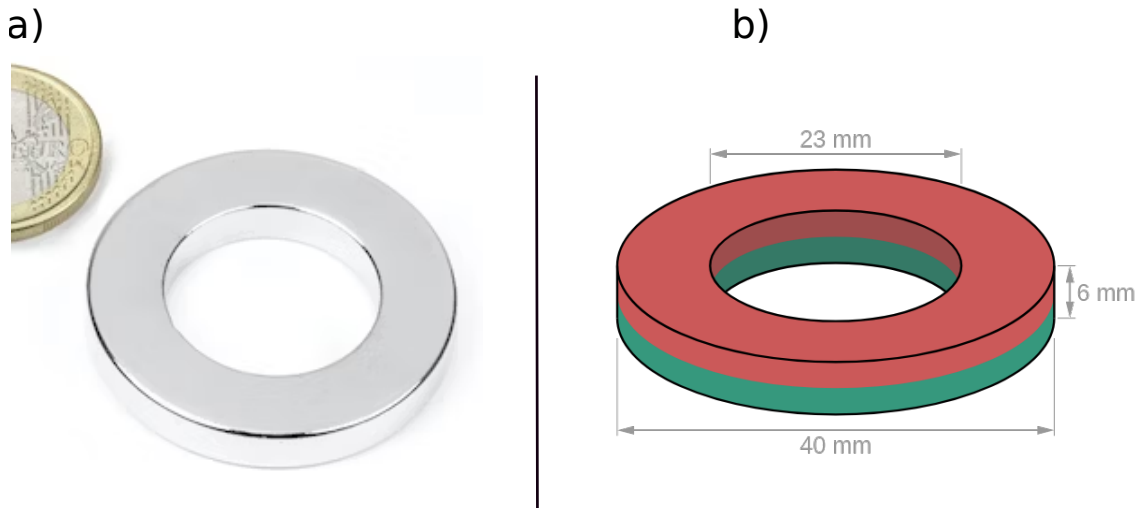


Figure 5.0.1: a) Image of a ring magnet, b) Poles and dimensions of a ring magnet — Images extracted from https://www.supermagnete.gr/ring-magnets-neodymium/ring-magnet-40mm-23mm-6mm_R-40-23-06-N

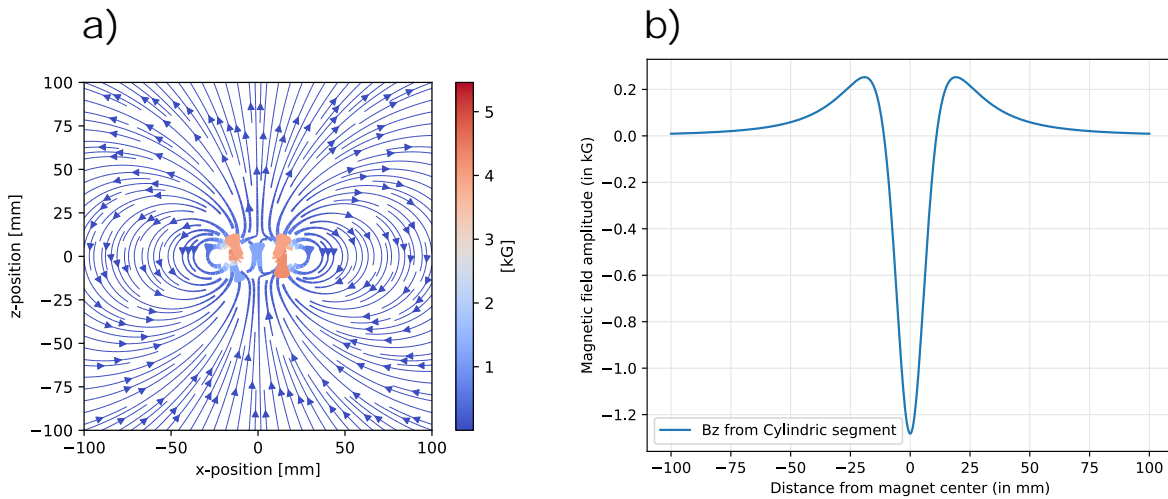


Figure 5.0.2: a) Map of the magnetic field created by a ring magnet along a diametrical cut, b) Magnetic field along the axis of the cylinder of a ring magnet — Simulation made with *Magpylib* [16]

Helmutz configuration and experimental verification

Our first idea for the study of the Faraday effect was to use an homogeneous magnetic field. For this we used an equivalent of the Helmutz configuration. Using the simulations, we found that the larger length on which the magnetic field can be homogeneous with such a configuration is with six magnets separated by 4 cm from six other magnets (the setup is represented in figure 5.0.3.a)). The experimental data points were taken with a magnetic field probe. The simulation data were re-scaled by a multiplicative coefficient to fit the experimental data. We see the simulation and the experimental data are in good agreement which motivates us to trust our simulations.

One side magnet only

For the following study, we found it easier to use only six magnets stuck together. Indeed we did not observe any critical deformation of the Faraday effect signal because of the inhomogeneous field. The zero crossings are still exploitable (see figure 4.2.2.c)). In the rest of this study most of the data were taken with a six magnets ring. The magnetic field produced by six stuck magnets is presented in figure 5.0.4. According to the distance from the magnets to the cell, the energy levels of the atoms will experience a mix of Paschen-Back effect and normal Zeeman effect.

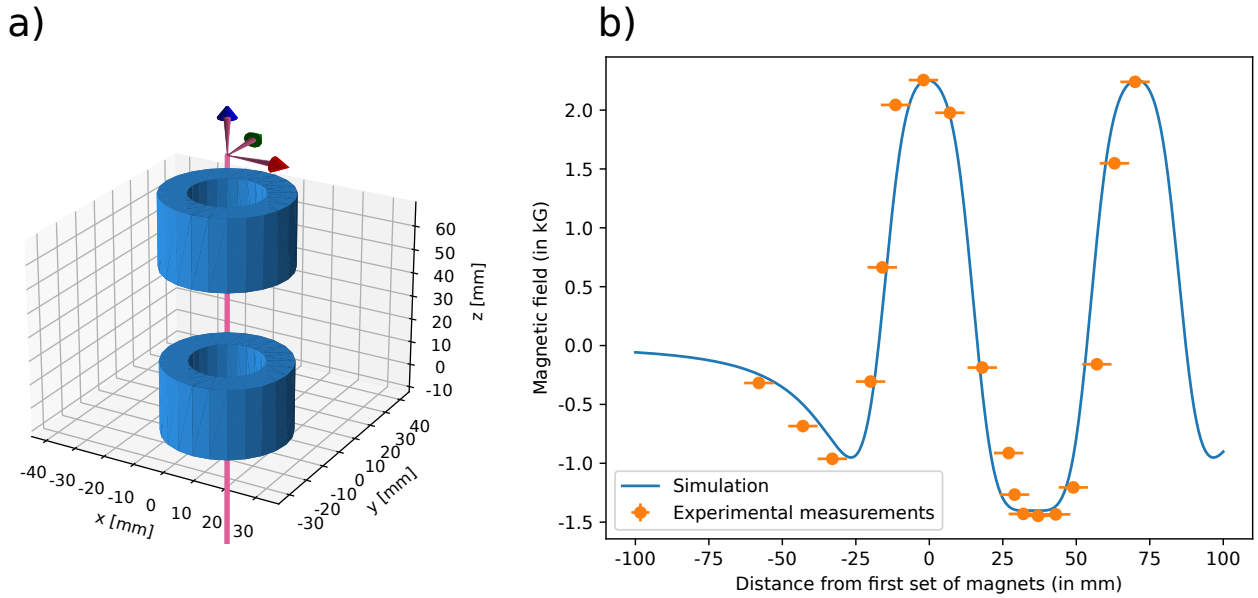


Figure 5.0.3: a) Experimental setup for the pseudo-Helmholtz configuration, b) Comparison between simulation and experiment for the amplitude of the magnetic field along the axis of the cylinder of a ring magnets

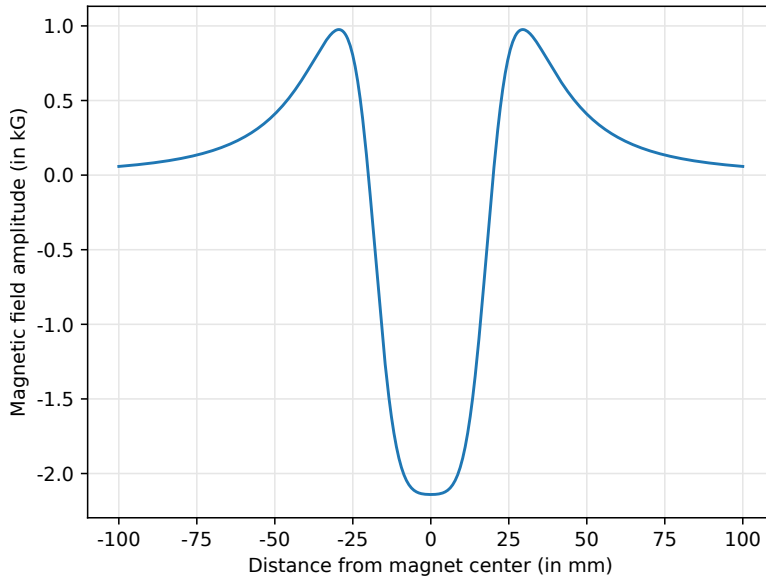


Figure 5.0.4: Simulation of the magnetic field along the axis of the cylinder of a ring magnets for 6 magnets stuck together

6 Evaluating the stability of the zero crossings of the Faraday effect

In this section, we will characterize the stability of the zero crossings of the Faraday effect we could get with our system. Then, it will allow us to know how stable we can expect our lock to be.

6.1 A tool, the Allan variance

In order to characterize the stability of the zero crossings we will recover the frequency positions of these zero crossings at different moments in time. In order to evaluate how the frequency shifts across time we will use a tool, the Allan variance [19][20]. The Allan variance allows us to know how stable the system is on different time scales. Indeed, the Allan variance is a function of a time scale, while when we compute the variance of a set of value we only get one value. Moreover this only value that is the variance can be biased by a constant shift in the frequency while on short time scales the system can be quite stable.

Let's say we have a sampling time of t_0 . For each sample we recover a frequency value, ω_k , of the lock point we want to study. For a time scale of $T = nt_0$ (scale on which we want to know the stability of the system), we define clusters (see the different colors on figure 6.1.1 for $T = 3t_0$). For each cluster, labeled i we define a mean frequency of $\Omega_i(T = nt_0) = \langle \omega_k \rangle_{k \in \{int_0, \dots, (in+n-1)t_0\}}$. We define the non overlapping Allan variance as in equation 6.1.1

$$\Omega_i(T = nt_0) = \langle \omega_k \rangle_{k \in \{int_0, \dots, (in+n-1)t_0\}}$$

$$\sigma_{\text{Non overlapping Allan}}^2(T) = \frac{1}{2} \langle (\Omega_{i+1}(T) - \Omega_i(T))^2 \rangle_i \quad (6.1.1)$$

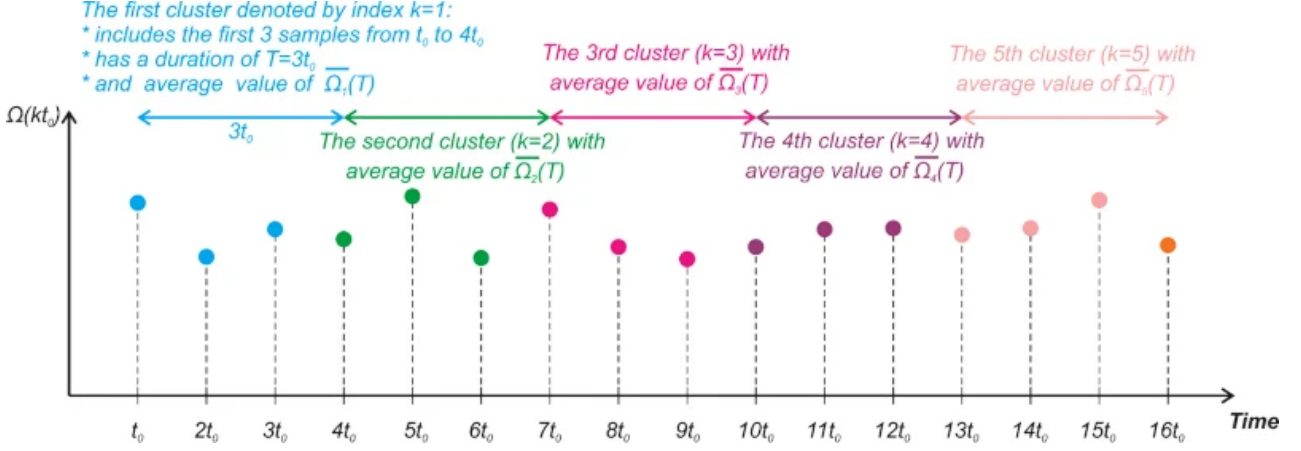


Figure 6.1.1: Representation of how to compute the non-overlapping Allan variance — Figure extracted from [19]

As explained previously, we see that the Allan variance allows us to know how stable the system is on a given time scale.

It also exists an overlapping definition of the Allan variance. Instead of defining clusters such that $\Omega_i(T = nt_0) = \langle \omega_k \rangle_{k \in \{int_0, \dots, (in+n-1)t_0\}}$, we define the clusters such that $\Omega_i(T = nt_0) = \langle \omega_k \rangle_{k \in \{it_0, \dots, (i+n-1)t_0\}}$ (see the cluster belonging with the color bars under the orange dots on figure 6.1.2). Thus, a sample ω_k belongs to several clusters. The overlapping Allan variance is then defined as in equation 6.1.2

$$\Omega_i(T = nt_0) = \langle \omega_k \rangle_{k \in \{it_0, \dots, (i+n-1)t_0\}}$$

$$\sigma_{\text{Overlapping Allan}}^2(T = nt_0) = \frac{1}{2} \langle (\Omega_{i+n}(T) - \Omega_i(T))^2 \rangle_i \quad (6.1.2)$$

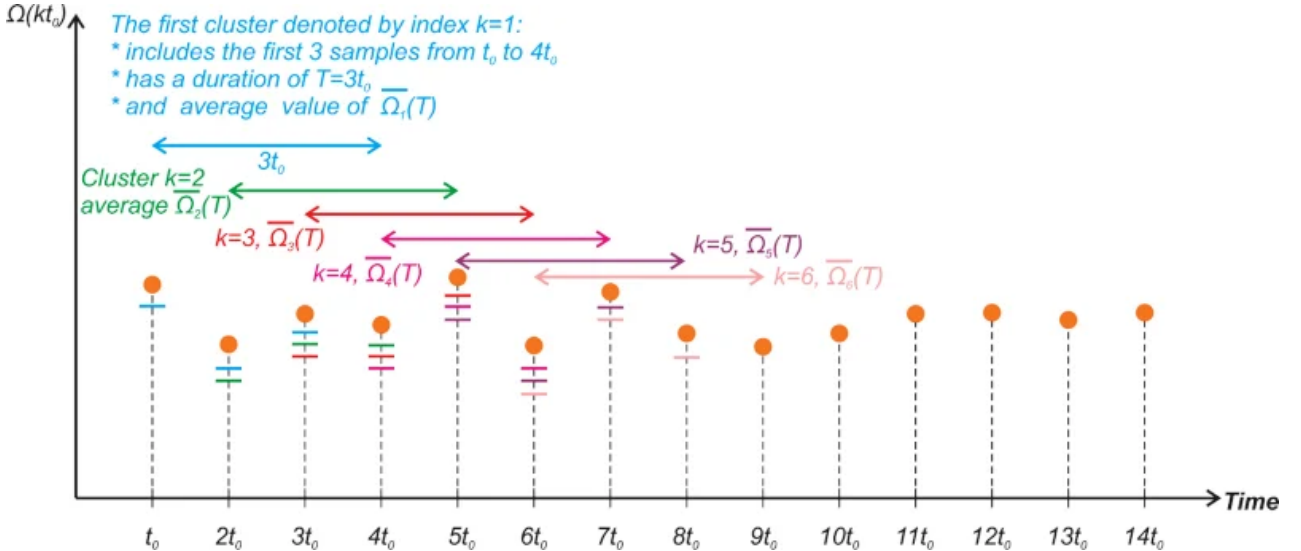


Figure 6.1.2: Representation of how to compute the overlapping Allan variance — Figure extracted from [19]

This is this definition of the Allan variance, we will use in the following report.

What we call a deviation is the square root of a variance.

6.2 Experimental setup

For this part of the study, we used the setup presented in figure 6.2.1.

In yellow is the Faraday effect system presented previously. In blue is a setup for a *Saturated absorption spectroscopy* (SAS). The balanced photo-diode is presented in A.2. A SAS is an absorption spectroscopy [21] where the thermal

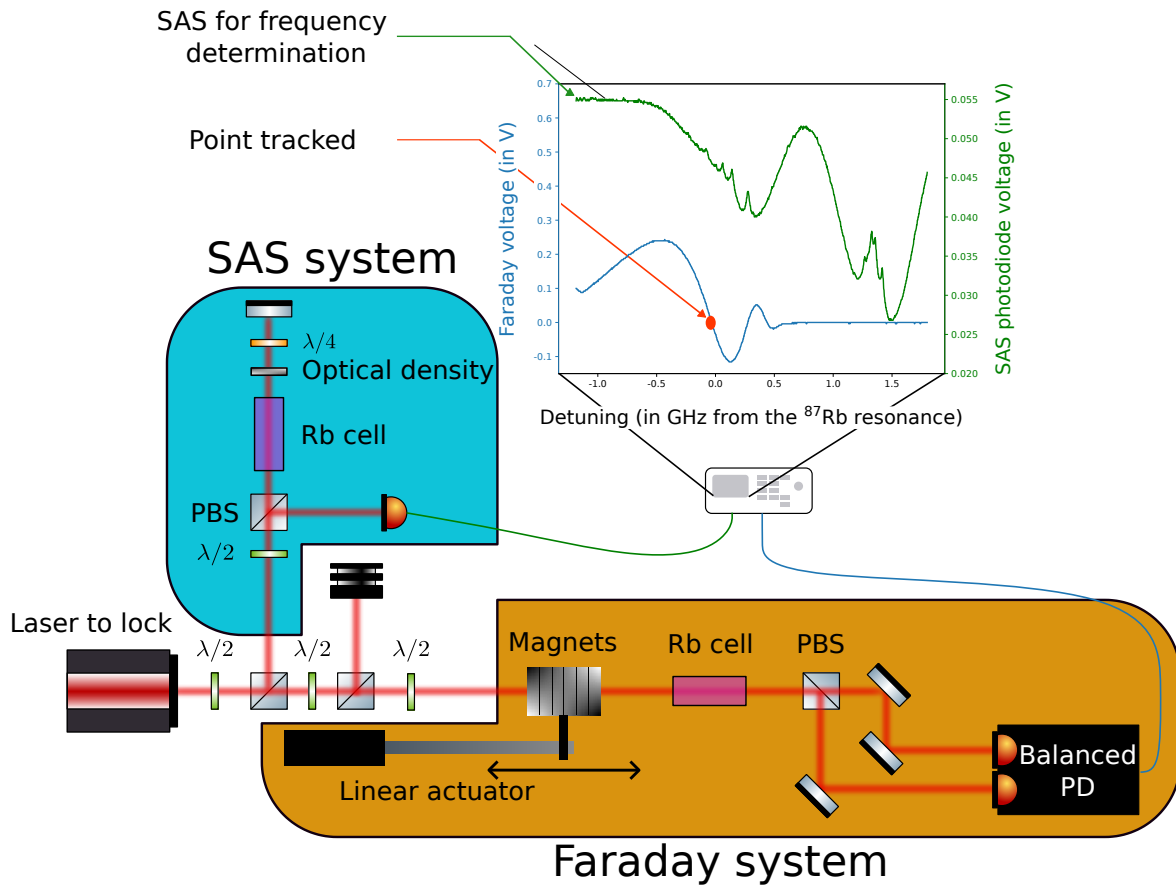


Figure 6.2.1: Setup for the frequency determination of the zero crossings of the Faraday effect

Doppler effect if exploited to make appear extremely thin transmission windows around the exact frequency of a transition and between two transitions (at the exact middle frequency).

In order to know where the zero crossings of the Faraday effect are located in frequency, we scan the laser frequency, here a Toptica laser diode (scanning with the piezoelectric). This same laser is sent to the SAS setup and to the Faraday setup. Voltages from the SAS diode and the Faraday balanced photo-diode are both acquired at the same time by an oscilloscope.

We then recover a time dependent transmission spectrum of the SAS system. This spectrum can be adjusted to an expected transmission spectrum (from theoretical values taken from [22]) (this adjustment is made for each sample (different nt_0)). An example of such an adjustment is presented in figure 6.2.2. Thanks to this adjustment we can recover a time to frequency dependence. With this method, the error on the frequency determination is around 10-20 MHz (this is a systematic error, on the absolute frequency).

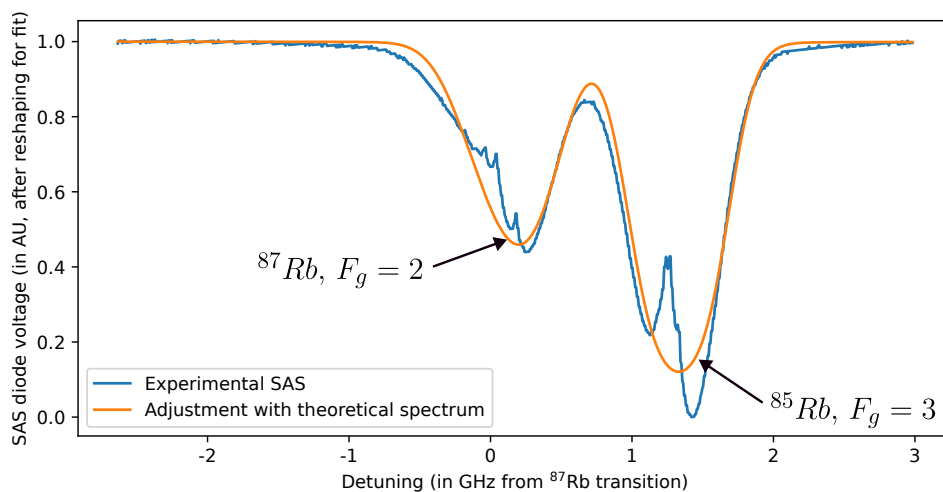


Figure 6.2.2: Example of an adjustment of the SAS for the D2 line in order to deduce the time/frequency dependence of the laser

Thus, we know the value of the voltage from the balanced photo-diode of the Faraday effect for each frequency.

With an algorithm we wrote it is possible to recover the frequency of this zero crossings and to sample this frequency at different moments in time in order to know how the frequency of this zero-crossing evolves (see annex C).

The Rubidium cell was typically warmed up to 100°C (according to an adjustment, see Annex B) and the power entering the Faraday system was about 10mW.

Our stability criteria for the Faraday effect zero crossings are a maximum excursion of 50MHz, with an Allan deviation of less than 25MHz on 30min-1hour time scales.

6.3 Results

In figure 6.3.1 are represented the results of two long stability runs (around one our each). The positions of the zero crossings are represented in figures 6.3.1.a) and 6.3.1.c). It is important to note that the magnetic field did not evolve in time in this study.

Figure 6.3.1.a) is a run where the temperature of the room was steady and nobody opened or closed the door. The standard deviation of the position of the zero crossing studied is of 4MHz. The overlapping Allan deviation (Figure 6.3.1.b)) is only declining which suggest a quite stable frequency of the zero crossing. This is this kind of stability we could get when the temperature of the room was steady.

Figure 6.3.1.c) is a run launched before a lunch, so the door was opened a lot and the pressure on the AC system was fluctuating. The standard deviation of the position of the zero crossing studied is of 12MHz and the maximal excursion was of 50MHz. The overlapping Allan deviation (Figure 6.3.1.d)) declines and then goes up again for clusters longer than 100s. This means that on time scales of the order of the minute, the system is stable. On longer time scales the frequency shifted. We think that this is due to changes on the temperature of the room (the effect on the position on frequency of the zero crossings is explained in 4.2.2). This is this kind of stability we got when the temperature of the room was fluctuating. These were rare cases. We expect the maximum of the overlapping Allan deviation to be under 25MHz which was what we had on this run.

We did not have the time to quantify how the temperature of the room really influences the position in frequency of the zero crossings.

We tried to maximize the isolation of the cell to reduce its temperature fluctuations.

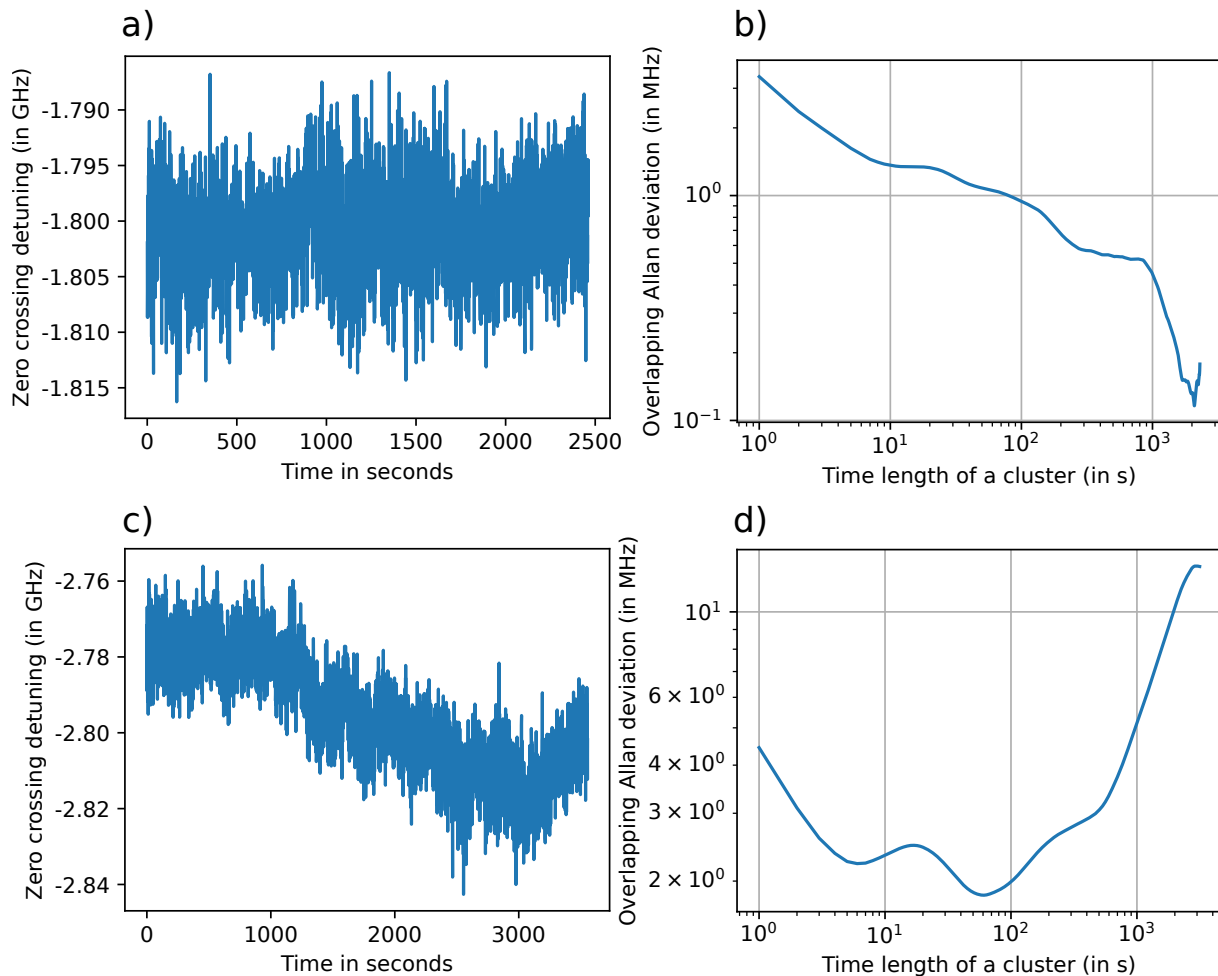


Figure 6.3.1: a) Excellent stability run, frequency representation, b) Overlapping Allan deviation of a), c) Bad stability run, d) Overlapping Allan deviation of c)

We agreed on the goodness of these stability characteristics.

7 First locks stability

Now that we have determined that the Faraday system is suitable for what we want to do, we will lock a laser on one of its zero crossings and determine the stability of this lock.

7.1 Experimental setup

In order to determine the frequency of the locked laser, we will use an other laser (locked on a known frequency) that will beat with the Faraday locked laser. The experimental setup to do so is presented in figure 7.1.1.

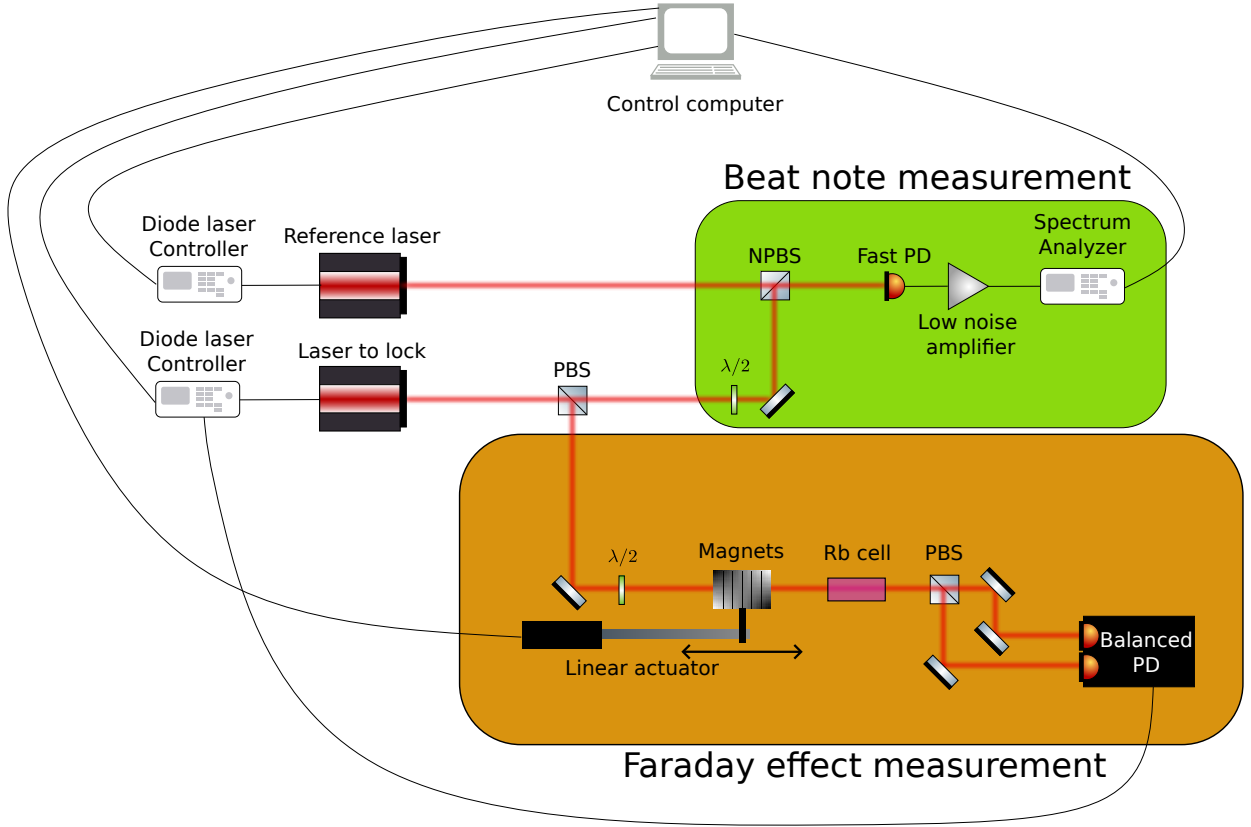


Figure 7.1.1: Experimental setup for evaluating the stability of the laser lock

The reference laser was locked on a crossover (D2 line, ^{87}Rb , $F_g = 2 \rightarrow F_f = 3$) of a saturated absorption setup (not shown on figure 7.1.1).

The laser to lock was split by a beam splitter. One part of its power was sent to the Faraday effect system with a constant magnetic field in time (see the orange box in figure 7.1.1). The voltage of the balanced photo-diode is the Faraday signal that is sent to the controller of the laser to lock on the Faraday effect. With the appropriate software and hardware (both supplied by Toptica) we could lock the laser on a zero crossing of the Faraday signal.

When the laser was locked, the other part of its power was recombined with some power of the reference laser to interfere and obtain a beat note. The beat note comes from the fact that $e^{i\omega_a t} + e^{i\omega_b t} = 2e^{i\frac{\omega_a + \omega_b}{2}t} \cos(\frac{\omega_a - \omega_b}{2}t)$. The resulting light of the superposition of the two laser beams of pulsation ω_a and ω_b is a light of pulsation $\frac{\omega_a + \omega_b}{2}$ and modulated at a pulsation $\frac{\omega_a - \omega_b}{2}$. We can detect this modulating pulsation with a spectrum analyzer.

We had to carefully manage the polarization of the laser locked with the Faraday effect (in order to match the polarisations of the two lasers and maximize the beat note signal). The two beam were carefully superposed (same propagation direction) and this beam composed of the two laser beams was focused on a fast photo-diode (Thorlabs DET08CL). The signal of this photo-diode was then amplified by a low noise amplifier (Mini-Circuits ZX60-14LN-S+). This signal was then analyzed by a high bandwidth Spectrum Analyzer (Agilent E4405B 13.2GHz bandwidth Spectrum Analyzer). This spectrum analyzer has been interfaced during this internship (see Annex A.3)

7.2 Results

A run of almost two hours was recorded with the experimental setup presented in 7.1. The evolution in time of the beat note of the two locked lasers is presented in figure 7.2.1.a), the standard deviation is of 5MHz. An example of

the power repartition in frequencies of the beat note signal is presented in 7.2.1.c). We see that the beat note signal is of more than 20dBm and has a Full Width at Half Maximum (FWHM) of approximately 5MHz.

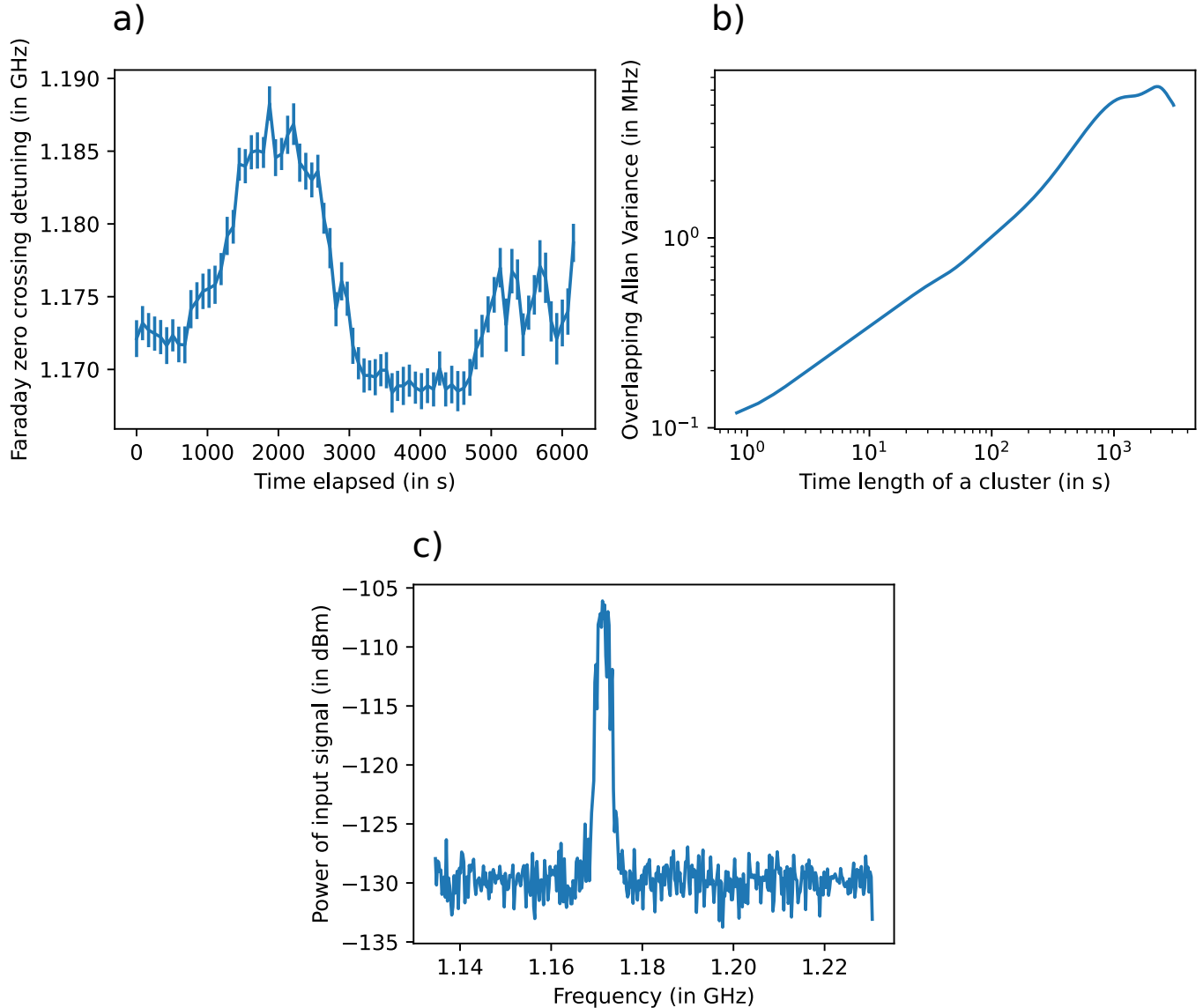


Figure 7.2.1: a) Evolution of the beat note frequency with time during the lock, b) Overlapping Allan deviation of the run presented in a), c) An example of the signal of the beat note on the spectrum analyzer

In figure 7.2.1.a), we notice that the beat note frequency jitters of less than 10MHz (which means a jitter of less than 20MHz for the relative frequency $|\omega_a - \omega_b|$). This jitter can either come from the frequency of the laser reference or from the frequency of the Faraday locked laser. Then there is obviously more jitter than if we only considered the frequency of the Faraday locked laser, what we can't do because we need a reference to know the frequency of the system. The overlapping Allan deviation reaches a plateau of approximately 5MHz and then seems to go down. On the time scale of one hour this is totally acceptable for the team.

We now know that the lock we can do with the Faraday effect corresponds to the needs of the team.

8 Tuning the zero crossings

Now that we know that the Faraday system is suitable for a locking error signal generation we need to be able to tune the frequency of the zero crossing. A first idea was to add a solenoid around the cell to slightly change the magnetic field. But we showed that it affected the stability of the system because the solenoid warms up when the current passing through it changes. In this section we then chose to move the magnets away of toward the cell to tune the magnetic field.

8.1 Using a linear actuator to move the magnets

We now go back to the experimental setup presented in 6.2. The magnets are mounted on a linear actuator presented in the orange box in figure 6.2.1. This linear actuator is described in A.4.

8.1.1 Reproducibility

By using the same method than the one described in 6.2 to determine the frequencies of the zero crossings we characterized the reproducibility of the zero crossing frequency for a certain motor elongation. This reproducibility test made by moving forward and then backward the motor are only valid on short period of time (not on days) because of the fluctuating room temperature on long times.

In figure 8.1.1 are represented the frequencies of the two first zero crossings of a Faraday effect. These points were taken by moving the motor, then measuring the frequencies of the zero crossings and then moving again. Two runs were made with 10 minutes waiting between them. During the first one, the motor was going forward, and during the second one, the motor was going backward.

Figure 8.1.1: Frequencies of the two first zero crossings of the Faraday effect when going forward, then waiting 10 minutes and then going backward

Taking into account the error bar we see that there is no hysteresis, on short time scales the movements of the motor seem reproducible. It should be enough to find the desired lock point and then stop moving the motor. We can change the frequency of a zero crossing by less than 10MHz, which is less than our stability criteria. We were able to reach detunings from -0.8GHz to -3.5GHz with the last pure 87, 5cm cell heated at 100°C.

8.1.2 Stability

Another problematic is whether the frequency of the zero crossings are stable after moving the motor. In order to know, we made a run where we moved the motor, characterized the stability, move the motor again, characterize and so on. The time evolution of the frequencies of the first zero crossing of a Faraday effect are represented in figure 8.1.2.a). The overlapping Allan deviations of each stability characterization (for one extension value) are all below 5MHz. Which means that moving the motor doesn't seem to affect the stability of the system.

Moreover, we made a longer stability characterization after having moved the motor. The time evolution of the frequency of the first zero crossing is presented in figure 8.1.2.b), its overlapping Allan deviation is represented in figure 8.1.2.c). We notice the system meets our desired stability criteria.

8.2 Setting the desired lock point

We now can tune the frequencies of the zero crossings. The final step of making a tunable lock system is to be able to set a desired lock frequency. In order to do so, we implemented an approach of the desired frequency by dichotomy [see the goto function](#). The frequencies were still determined with a SAS.

We move the motor between its minimal and maximal extension and record the zero crossings frequencies (We can recover more than one zero crossing, let's say k). The nearest we are from the resonance, the steepest the slope around the zero crossing will be and better the lock can be) of the Faraday effect for a certain number of points, let's say k . For each zero crossing we determine if it approaches the desired frequency when moving the motor. If more than one zero crossing can be tuned to the desired frequency, we will choose the zero crossing that has the steepest slope when it is near the desired frequency. Then we take again k points between the two extensions between which the desired frequency for the chosen zero crossing is located. We do so until we are less than 10MHz away from the lock point or when the k extension points are too near.

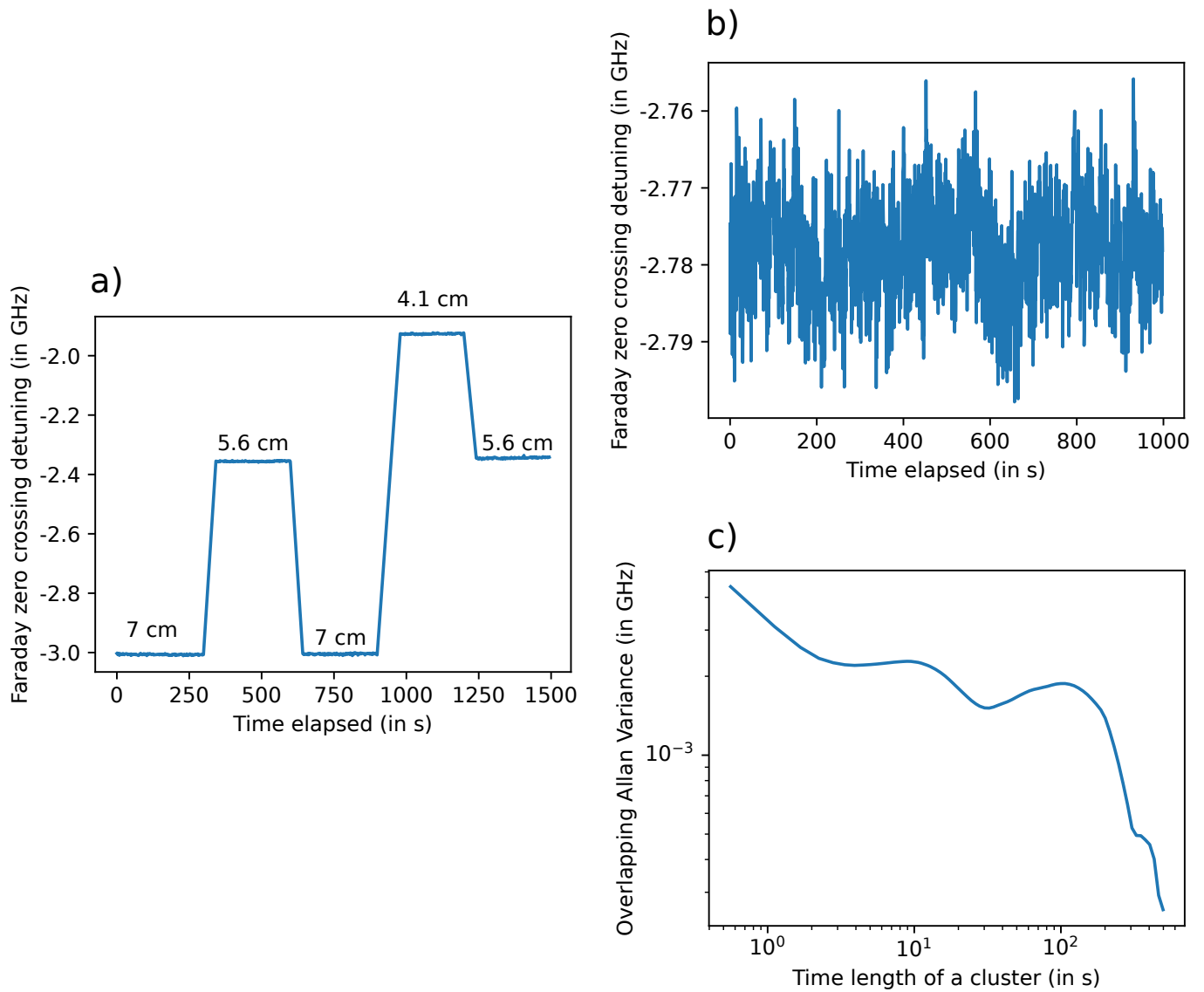


Figure 8.1.2: a) Frequency evolution of time of the first zero crossing of the system when modifying the extension of the actuator. The extensions of the motor are indicated, b) Long run after the movement of the motor, characterizing the stability of the frequency of the zero crossing, c) Overlapping Allan deviation, of b)

This system works quite well. In figure 8.2.1.a) is represented the Faraday effect signal obtained after having tuned one of its zero crossing to -1.4GHz from the D2 ^{87}Rb , $F_g = 2$ resonance. The reach frequency was -1.405GHz. The frequency evolution of this lock point and its Allan deviation are presented in figure 8.2.1 b) and c).

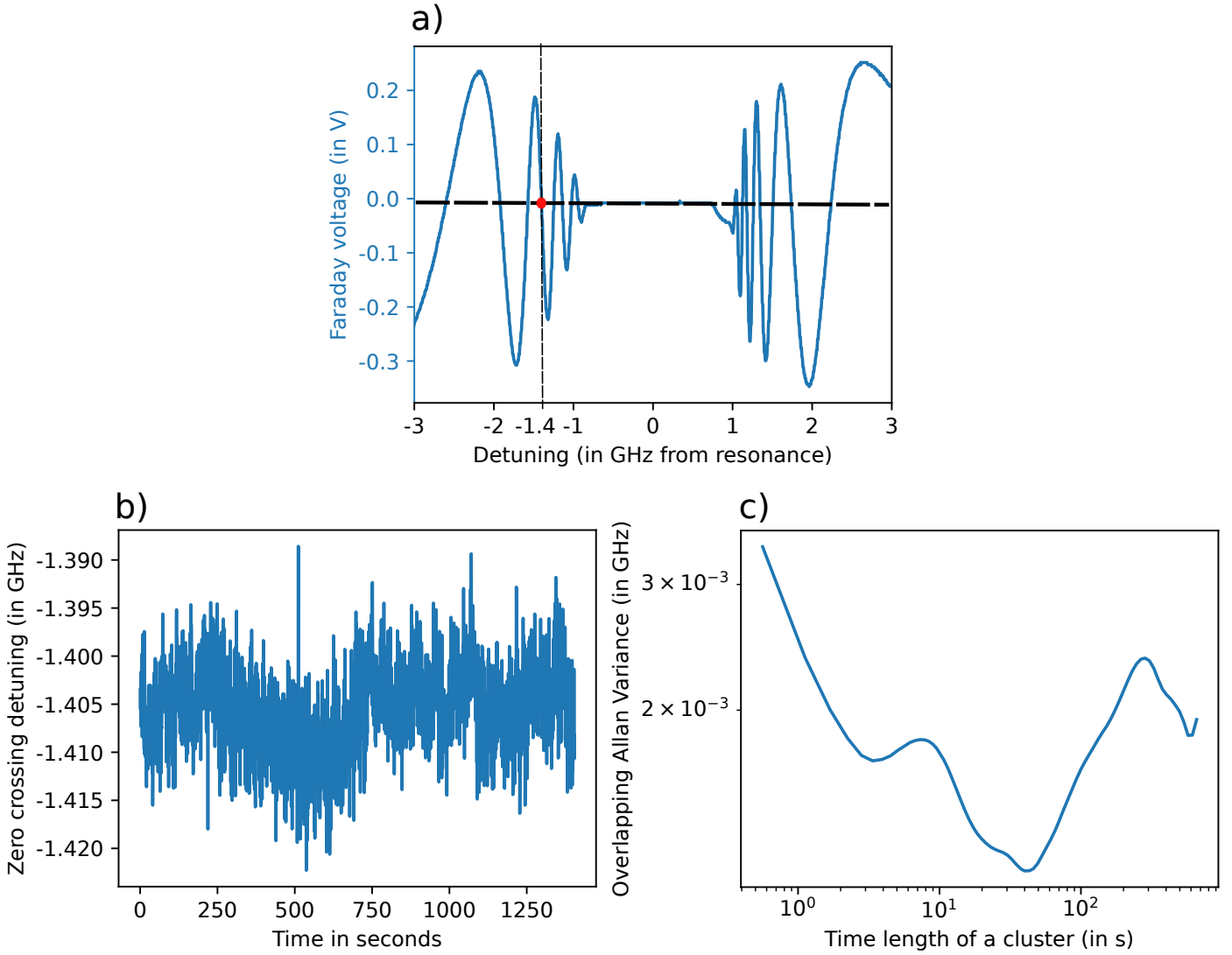


Figure 8.2.1: a) Faraday effect signal with a zero crossing tuned to be next to -1.4GHz from the D2 ^{87}Rb , $F_g = 2$ resonance, b) Time evolution of the frequency detuning of the zero crossing in red in a), c) Overlapping Allan deviation of b)

We notice that in figure 8.2.1.b) the mean frequency is steady in time (confirmed by the overlapping Allan deviation of less than 5MHz) and the excursion from the reached frequency is of 10MHz maximum. Then we can say that we reached the lock point and that the system meets the lock system's criteria.

9 Embedding the Faraday lock system in a box

We embedded the lock system in an all-in-one box. Its scheme is presented in figure 9.0.1. The laser beam of the laser to lock is sent to the box via an optical fiber. The box needs a SAS voltage of this same laser to be able to tune the zero crossings.

A Side activities

A.1 Designing holders for the magnets

I designed holders for the magnets and 3D printed them. What they look like is shown in figure A.1.1.

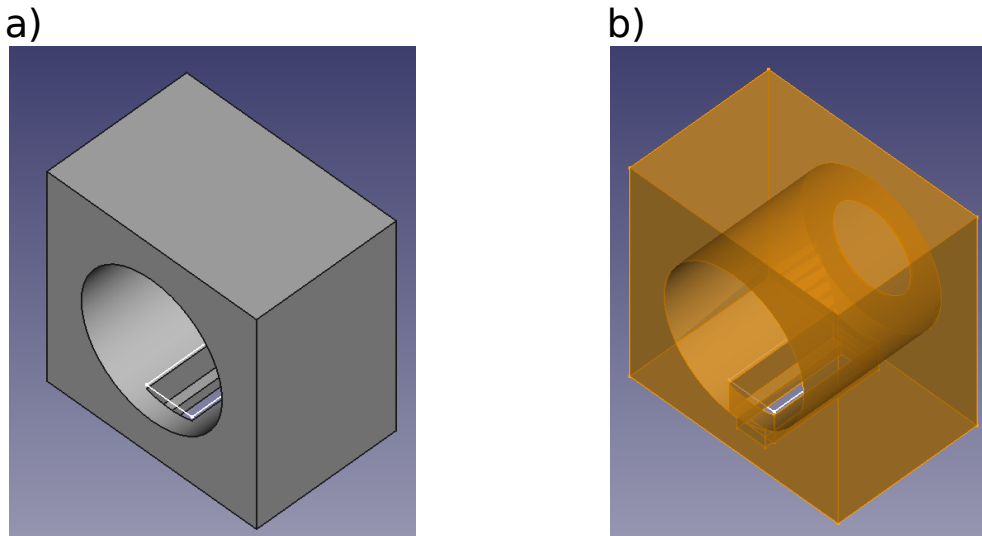


Figure A.1.1: a) View of the filled holder, b) View of the emptied holder

The file is available [here](#).

A.2 Home made balanced photo-diodes

I asked the electronic team to make a balance photo-diode. It has a 100MHz bandwidth. The balanced photo-diode used in this study has two outputs (A BF, frequencies until 10kHz, there is an internal offset to counter balance the dark current, and a HF, frequencies from 0Hz-100MHz. On this input with no light commit there is a non zero voltage because of the dark current). Their working principle is explained [here](#). [An other link to get insights about trans-impedance amplifiers](#).

A.3 GPIB to USB — Interfacing the Spectrum Analyzer

A GPIB-USB adapter was bought ([National Instrument GPIB-USB-HS+, USB 2.0, NI-488.2](#)). A tutorial has been written on how to connect to it to LINUX, it is available [here](#). The Agilent E4405B 13.2GHz bandwidth Spectrum Analyzer has been interface, the code is available [here](#).

A.4 Developing a python controlled continuous linear actuator

With a commercial linear actuator, I developed an electronic card to connect it to an Arduino and be able to control it with python. All the informations are available [on github](#). PCB cards were developed with the electronic team.

A.5 TENMA power source interface

I developed a python code to communicate with the TENMA 72-2715 power source. The code and some explanations in the README file are available on the group's GitHub : https://github.com/Quantum-Optics-LKB/Power_Supply_RS232_Control

A.6 Installing a router in the Rb room

I installed a new router in the Rb room, a [TP Link Archer C80](#). It's configuration page is accessed by the IP [192.168.0.100](#). The details of its DHCP server and the passwords are [on github](#).

B Cell's temperature determination

An adjustment was made to determine the temperature of the cell we worked with. We made a simple transmission spectrum for a very low entrance power (in order to avoid power broadening effects) and made an adjustment of this spectrum with a theoretical one. A result of such an adjustment is presented in figure [B.0.1](#).

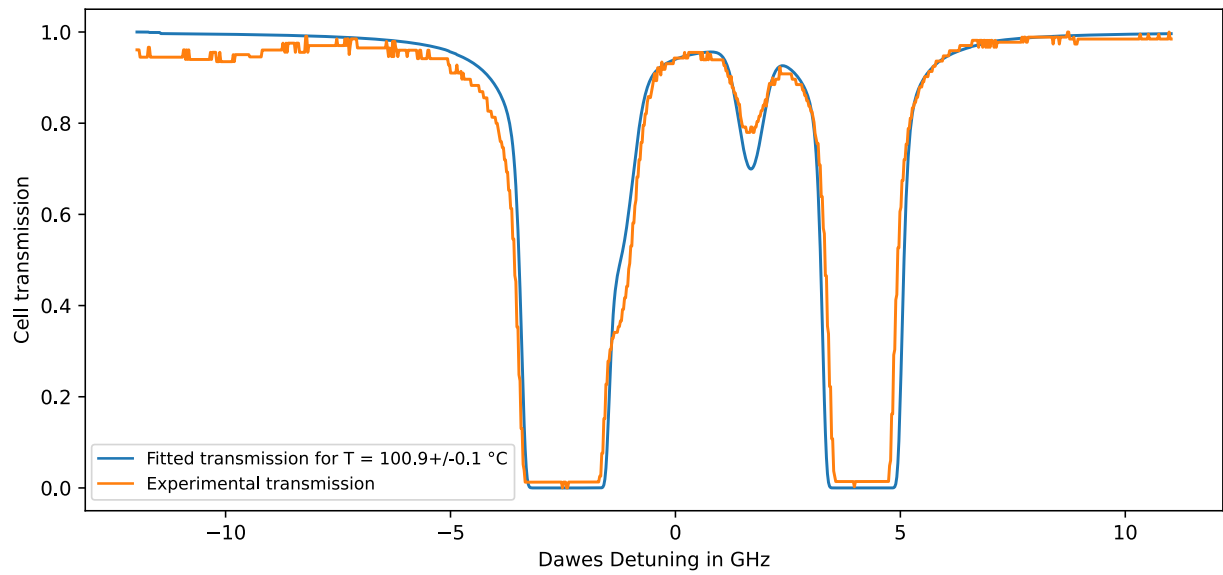


Figure B.0.1: Adjustment of the absorption spectrum of the Faraday cell in order to determine its temperature

C Coding for the Faraday study

A library of functions used to treat the Faraday effect was developed. They are available [here](#)

References

- [1] “Atomic Data for Rubidium (Rb).” [Online]. Available: <https://physics.nist.gov/PhysRefData/Handbook/Tables/rubidiumtable1.htm>
- [2] D. A. Steck, “Rubidium 85 D Line Data,” Sep. 2001. [Online]. Available: <https://steck.us/alkalidata/rubidium85numbers.pdf>
- [3] —, “Rubidium 87 D Line Data,” Sep. 2001. [Online]. Available: <https://steck.us/alkalidata/rubidium87numbers.1.6.pdf>
- [4] J.-P. Pérez, R. Fleckinger, and R. Carles, *Électromagnétisme, Fondements et applications, avec 300 exercices et problèmes résolus*, ser. HORS COLLECTION. Dunod, Jan. 2020. [Online]. Available: <https://www.dunod.com/sciences-techniques/electromagnetisme-fondements-et-applications-avec-300-exercices-et-problemes-0>
- [5] J. Raimond, “Atoms and photons,” Oct. 2013. [Online]. Available: <https://www.phys.ens.fr/IMG/pdf/m2icfpatomsphotons.pdf>
- [6] Q. Fontaine, “Paraxial fluid of light in hot atomic vapors,” phdthesis, Sorbonne Université, Jan. 2020. [Online]. Available: <https://tel.archives-ouvertes.fr/tel-03402487>
- [7] Q. Glorieux, “Quantum optics in dense atomic media: From optical memories to fluids of light.” [Online]. Available: <http://arxiv.org/abs/1812.08602>
- [8] F. Dalfovo, S. Giorgini, L. P. Pitaevskii, and S. Stringari, “Theory of bose-einstein condensation in trapped gases,” vol. 71, no. 3, pp. 463–512. [Online]. Available: <https://link.aps.org/doi/10.1103/RevModPhys.71.463>
- [9] P. B. H. Bransden and P. C. J. Joachain, *Physics of Atoms and Molecules*, 2nd ed. Harlow, England ; New York: Pearson, Apr. 2003.
- [10] S. L. Kemp, I. G. Hughes, and S. L. Cornish, “An analytical model of off-resonant faraday rotation in hot alkali metal vapours,” vol. 44, no. 23, p. 235004. [Online]. Available: <https://iopscience.iop.org/article/10.1088/0953-4075/44/23/235004>
- [11] A. L. Marchant, S. Haendel, T. P. Wiles, S. A. Hopkins, C. S. Adams, and S. L. Cornish, “Off resonance laser frequency stabilization using the faraday effect,” vol. 36, no. 1, p. 64. [Online]. Available: <http://arxiv.org/abs/1007.2531>
- [12] A. Millett-Sikking, I. G. Hughes, P. Tierney, and S. L. Cornish, “DAVLL lineshapes in atomic rubidium,” vol. 40, no. 1, p. 187. [Online]. Available: <https://dx.doi.org/10.1088/0953-4075/40/1/017>
- [13] S. Pustelny, V. Schultze, T. Scholtes, and D. Budker, “Dichroic atomic vapor laser lock with multi-gigahertz stabilization range,” vol. 87, no. 6, p. 063107. [Online]. Available: <http://aip.scitation.org/doi/10.1063/1.4952962>
- [14] T. Xiao, T. Wang, and B. Yan, “Note: A simple magnetic field design for dichroic atomic vapor laser lock,” vol. 89, no. 4, p. 046106, publisher: American Institute of Physics. [Online]. Available: <https://aip.scitation.org/doi/full/10.1063/1.5020519>
- [15] C. Lee, G. Z. Iwata, E. Corsini, J. M. Higbie, S. Knappe, M. P. Ledbetter, and D. Budker, “Small-sized dichroic atomic vapor laser lock (DAVLL),” vol. 82, no. 4, p. 043107. [Online]. Available: <http://arxiv.org/abs/1012.3522>
- [16] M. Ortner and L. G. Coliado Bandeira, “Magpylib: A free python package for magnetic field computation,” vol. 11, p. 100466. [Online]. Available: <https://www.sciencedirect.com/science/article/pii/S2352711020300170>
- [17] Q. L. Peng, S. M. McMurry, and J. M. D. Coey, “Axial magnetic field produced by axially and radially magnetized permanent rings,” vol. 268, no. 1, pp. 165–169. [Online]. Available: <https://www.sciencedirect.com/science/article/pii/S0304885303004943>
- [18] G. Lemarquand, V. Lemarquand, S. Babic, and C. Akyel, “Magnetic field created by thin wall solenoids and axially magnetized cylindrical permanent magnets.”
- [19] S. Arar. Introduction to allan variance—non-overlapping and overlapping allan variance - technical articles. [Online]. Available: <https://www.allaboutcircuits.com/technical-articles/intro-to-allan-variance-analysis-non-overlapping-and-overlapping-allan-variance/>
- [20] P. J. Sherman, “Allan variance.” [Online]. Available: <https://home.engineering.iastate.edu/~shermanp/AERE432/lectures/Rate%20Gyros/Allan%20variance.pdf>
- [21] “Saturated absorption spectroscopy.” [Online]. Available: https://www.phys.ufl.edu/courses/phy4803L/group_III/sat_absorbtion/SatAbs.pdf
- [22] A. M. Dawes, “Rubidium spectrum model,” original-date: 2011-11-30T18:46:36Z. [Online]. Available: <https://github.com/DawesLab/rubidium>